

MALAYSIAN JOURNAL OF ANALYTICAL SCIENCES



Journal homepage: https://mjas.analis.com.my/

Research Article

Innovative oil removal technology: Graphene oxide@ZIF-8 on alumina hollow fibre membranes

Dayang Norafizan Awang Chee^{1*}, Faezrul Zackry Abdul Halim¹, Muhammad Shamil Soffian¹, Nur Afiqah Kamaludin¹, Claudeareena Garlding¹, Mohamed Afizal Mohamed Amin², and Farhana Aziz³

Received: 7 May 2025; Revised: 17 July 2025; Accepted: 21 July 2025; Published: 29 August 2025

Abstract

Oily wastewater pollution poses a severe threat to freshwater resources, marine ecosystems, and human health. To address this, a graphene oxide (GO) based nanocomposite membrane integrated with Zeolitic Imidazolate Framework-8 (ZIF-8) was constructed on a pristine alumina (Al₂O₃) hollow fibre support. The resulting GO@ZIF-8/Al₂O₃ membrane exhibited a high surface area and abundant oxygen-containing functional groups, enhancing its oil adsorption and separation performance. GO was synthesized via a modified Hummers' method, followed by in situ solvothermal assembly with ZIF-8. The membrane structure was characterized using Fourier-Transform Infrared Spectroscopy (FTIR), Ultraviolet–Visible (UV–Vis) Spectroscopy, X-Ray Diffraction (XRD), and Field Emission Scanning Electron Microscopy (FESEM). Batch adsorption and crossflow filtration studies were performed to evaluate membrane performance. Adsorption data fit well to the Freundlich isotherm model (R² = 0.98046) and pseudo-second order kinetics (R² = 0.98247), indicating multilayer chemisorption. The GO_(2:1)@ZIF-8/Al₂O₃ membrane achieved up to 96.32% oil removal and maintained 90.08% rejection after six reuse cycles. Compared to the pristine membrane, which showed only 33.65 Lm⁻²h⁻¹ flux, the modified membrane achieved 92.15 Lm⁻²h⁻¹, a 173.9% improvement. These findings demonstrate a robust and reusable membrane system with excellent potential for practical oily wastewater treatment.

Keywords: graphene oxide, membrane, oil removal, reusability, zeolitic imidazoalate framework-8

Introduction

Access to clean water is essential for industrial operations, agriculture, and human health. Although water covers approximately 71% of the Earth's surface, only around 3% is freshwater, and less than 1% is readily accessible due to factors such as glacial entrapment and pollution [1,2]. Among these pollutants, oily wastewater has become a major concern, especially from the automotive, palm oil, and oil field industries [3]. The oil and gas industry, in particular, contributes significantly to this issue by generating large volumes of oily wastewater, worsening the global water crisis. By 2025, nearly 66% of the global population is expected to live in areas facing significant water scarcity [4].

The treatment of oily wastewater remains technically challenging due to the complex mixture of dispersed oil droplets and surfactants [5]. Regulatory limits stipulate that total oil and grease in treated water should remain below 10-15 mg/L, while untreated industrial effluents may exceed 1000 mg/L [6,7]. Conventional methods such as chemical precipitation, flocculation, biological treatment, electrocoagulation often struggle to achieve efficient separation [8,9]. As a result, membrane-based filtration technologies have gained attention due to selective separation capabilities, energy efficiency, and reduced chemical usage. Ceramic membranes, especially those based on alumina hollow fibres, offer several advantages over polymeric membranes, including thermal and chemical stability,

¹Faculty of Resource Science and Technology, Universiti Malaysia Sarawak, 94300 Kota Samarahan, Sarawak, Malaysia

²Department of Chemical Engineering and Energy Sustainability, Faculty of Engineering, Universiti Malaysia Sarawak, 94300 Kota Samarahan, Sarawak, Malaysia

³Advanced Membrane Technology Research Centre (AMTEC), School of Chemical and Energy Engineering, Faculty of Engineering, Universiti Teknologi Malaysia, Johor Bahru, 81310 Johor Darul Takzim, Malaysia

^{*}Corresponding author: dnorafizan@unimas.my

mechanical strength and longer operational lifespans [10,11]. However, membrane fouling, especially by oil and insufficient surface functionality, limits their oil separation performance [12].

One of the key challenges in alumina-based membrane filtration lies in the poor oil adsorption capacity due to a lack of surface functional groups and weak interactions between the ceramic surface and oil droplets. Additionally, poor separation efficiency caused by inadequate surface modification can compromise membrane performance in real-world applications. To overcome these issues, researchers have turned to surface functionalization using carbon nanomaterials such as graphene oxide (GO). GO is a highly hydrophilic nanomaterial with abundant oxygen-containing groups that facilitate oil adsorption by increasing surface energy and offering multiple active sites [13,14]. However, GO membranes suffer from structural instability in aqueous environments, where they tend to delaminate or disintegrate over time [15].

To address GO's stability issue, the hybridization of GO with metal-organic frameworks (MOFs), such as Zeolitic Imidazolate Framework-8 (ZIF-8), offers a promising solution. ZIF-8 is known for its large surface area, uniform nanoporous structure, and chemical stability, making it highly suitable for use in separation membranes [16]. When incorporated with GO, ZIF-8 helps prevent GO disintegration by forming stable chemical interactions such as hydrogen bonding and coordination bonds while also enhancing the composite's overall adsorption capacity and stability [17,18]. Moreover, ZIF-8 helps reduce particle agglomeration by uniformly distributing onto the GO nanosheets, further improving membrane performance.

While previous studies have explored either GO or ZIF-8 separately for oily wastewater treatment, few have demonstrated the integration of both onto a ceramic support via a simple, scalable method. This work distinguishes itself by combining GO's surface functionality with ZIF-8's structural robustness to form a hybrid membrane on a hollow fibre alumina support [19]. This design not only improves oil adsorption and separation efficiency but also enhances membrane stability in aqueous environments, an issue that limits the long-term usability of conventional GO membranes [20].

Unlike previous studies that explore either GO or ZIF-8 individually or use simple drop-casting methods, our work introduces a one-step in-situ solvothermal synthesis to grow GO@ZIF-8 directly onto an alumina hollow fibre, achieving a tightly bound composite layer with improved structural integrity.

Additionally, we compare two formulations, GO:ZIF-8 ratios of 1:1 and 2:1, to investigate the effect of composition on separation performance and reusability.

Therefore, the objective of this study is to synthesize, characterize, and evaluate the oil removal performance of a GO@ZIF-8/Al₂O₃ nanocomposite membrane. Characterization was conducted using FTIR, XRD, UV-Vis, and FESEM, while performance was assessed through batch adsorption, kinetic and isotherm modeling, and crossflow filtration studies. The results provide insights into the composite membrane's efficiency, stability, and scalability for practical oily wastewater treatment applications.

Materials and Methods Materials

Graphite powder (Sigma-Aldrich) served as the starting material for graphene oxide (GO) synthesis. Additional reagents included concentrated sulphuric acid (98% H₂SO₄), sodium nitrate (NaNO₃), potassium permanganate (KMnO₄), hydrogen peroxide (30% H₂O₂), and hydrochloric acid (35% HCl). All equipment and glassware were pre-cleaned using detergent and thoroughly rinsed with deionized (DI) water.

For APTES surface modification, toluene (ACS reagent, Merck) and 3-(aminopropyl)triethoxysilane (APTES, 99%, Sigma-Aldrich) were used. Preparation of the GO@ZIF-8/Al₂O₃ membrane involved N,N-Dimethylformamide (DMF, Merck), 2-methylimidazole (2-MeIM, 99%, Sigma-Aldrich), zinc nitrate hexahydrate (Zn(NO₃)₂·6H₂O, 98%, Sigma-Aldrich), and sodium formate.

Preparation of graphene oxide

Graphene oxide (GO) was synthesized from graphite powder using a modified version of Hummers' method [21,22]. Initially, 23 mL of concentrated sulphuric acid (98%) was cooled below 0°C using an ice bath. A separate mixture of 1 g of graphite and 0.5 g of sodium nitrate was then gradually introduced into the chilled acid under constant stirring for 45 minutes. Following this, 3 g of potassium permanganate was added slowly while maintaining the temperature below 20°C. The solution changed colour, indicating successful oxidation and was stirred for an additional 15 minutes as shown in **Figure 1**.

After this, the mixture was removed from the ice bath and allowed to warm to room temperature. As the solution changed to brown, 140 mL of DI water was added slowly. To terminate the reaction, 10 mL of 30% H_2O_2 was added, followed by 15 minutes of stirring. The resulting suspension was filtered and repeatedly washed with 5% HCl solution until no sulphate ions

were detected using 0.2 M BaCl₂. The product was then rinsed with DI water until the pH was in the range of 5–6.

Preparation of GO@ZIF-8 alumina membrane alumina hollow fibre membrane modification using 3-aminopropryl triethoxysilane (APTES)

The alumina hollow fibre membranes were cleaned by ultrasonication for 5 minutes in methanol, acetone, and DI water. Following this, the membranes were immersed in 2% APTES in toluene and silanized for 2 hours to introduce amine groups [23]. After modification, the membranes were rinsed with ethanol and dried at 60°C for 30 minutes to remove surface solvents.

Preparation of GO@ZIF-8 composites

Zn(NO₃)2•6H₂O, 2-MeIM, and sodium formate were mixed in a molar ratio of 1:2:1:313 using DMF as the solvent. Specifically, 0.3 g of Zn(NO₃)2•6H₂O was dissolved in 31.3 mL of DMF to form the metal precursor. In parallel, 0.6 g of 2-MeIM and 0.3 g of sodium formate were dissolved in 62.6 mL of DMF to create the ligand solution. Graphene oxide sheets were added to the ligand solution in fixed ratios relative to the zinc precursor: 0.3 g GO for the 1:1 formulation

and 0.6 g GO for the 2:1 formulation, corresponding to GO:Zn weight ratios of 1:1 and 2:1, respectively. The mixture was then ultrasonicated for 30 minutes to ensure uniform dispersion of the GO sheets [24]. This mixture was stirred for an additional 2 hours before slowly adding it to the metal precursor under vigorous stirring, yielding a cloudy suspension of GO@ZIF-8 as shown in **Figure 2**. The procedure was repeated for the 2:1 formulation using 0.6 g GO, while all other precursor amounts and conditions were kept constant as shown in **Table 1**.

The GO:Zn weight ratios of 1:1 and 2:1 were selected to assess the influence of GO loading on membrane structure and oil separation performance. The 1:1 formulation served as a baseline, while the 2:1 formulation tested whether increased GO content could enhance surface functionalization, adsorption sites, and hydrophilicity. These ratios were chosen based on prior studies that reported performance improvements with moderate GO increases, provided dispersion and structural integrity were maintained [16, 25]. The resulting membranes are referred to as $GO_{(1:1)}@ZIF-8/Al_2O_3$ and $GO_{(2:1)}@ZIF-8/Al_2O_3$ and were used in all subsequent characterizations and separation studies.

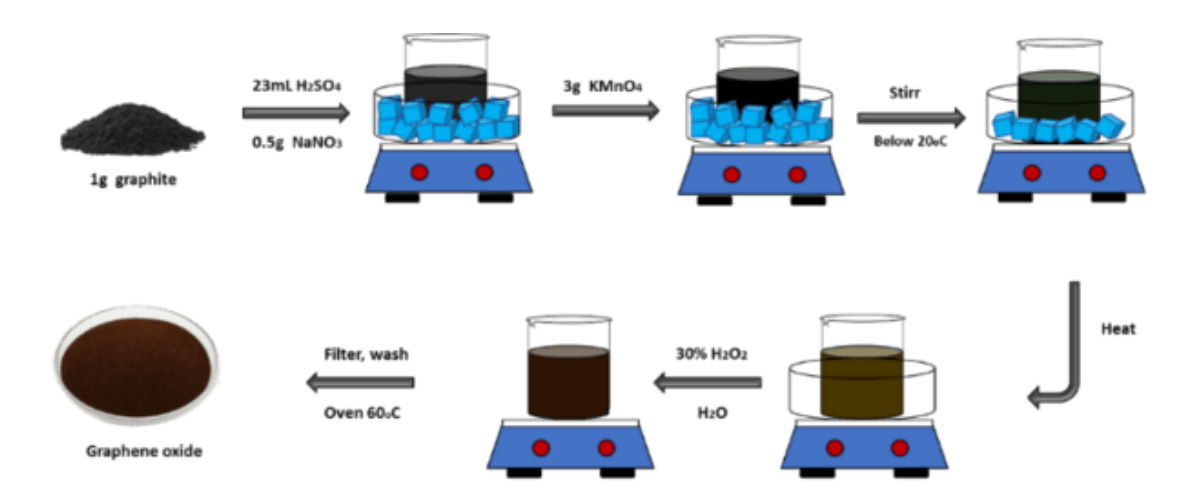


Figure 1. Schematic diagram of GO synthesis

Table 1. Prepared membrane samples with corresponding GO:Zn ratios

Membrane Sample	GO Amount	Zn(NO ₃) ₂ ·6H ₂ O Amount	GO:Zn Ratio
	(g)	(g)	(w/w)
Pristine Al ₂ O ₃	_	_	_
$GO_{(1:1)}@ZIF-8/Al_2O_3$	0.3	0.3	1:1
$GO_{(2:1)}$ @ZIF-8/Al ₂ O ₃	0.6	0.3	2:1

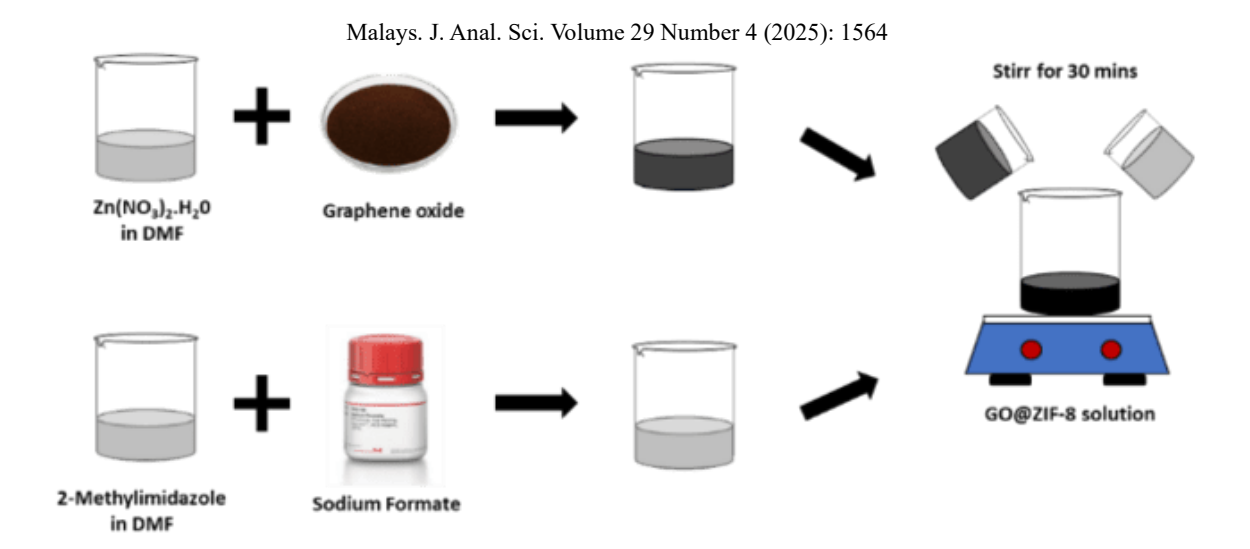


Figure 2. GO@ZIF-8 synthesis solution

GO@ZIF-8/Al₂O₃ membrane prepared in situ by solvothermal

To prevent the infiltration of synthesis solution into the membrane lumens, both ends of the APTES-modified alumina fibres were sealed with PTFE tape, then placed in a Teflon-lined autoclave filled with the GO@ZIF-8 suspension and heated at 130°C for 24 hours. After synthesis, the membranes were washed with DMF and dried at 60°C for 4 hours to remove residual solvents, as shown in **Figure 3**.

Characterizations

The physical and chemical characteristics of the GO@ZIF-8/Al₂O₃ membranes were thoroughly evaluated using a series of analytical techniques. Field emission scanning electron microscopy (FESEM, JEOL JSM-IT500HR) was used to observe both surface and cross-sectional morphologies of the membranes. Membrane samples were cut to approximately 0.5 cm in length and mounted on platinum stubs, followed by a thin gold–platinum sputter coating under vacuum (20 mA, 3 minutes) to minimize charging effects during imaging. For nanocomposite characterization, a pristine GO and GO@ZIF-8(1:1) sample was used to examine the surface morphology of the synthesized material before membrane coating.

Fourier-transform infrared spectroscopy (FTIR, Thermo Nicolet IS10) was employed to identify surface functional groups. The GO@ZIF-8(1:1) nanocomposite was finely ground, blended with potassium bromide (KBr), and compressed into pellets before scanning across a range of 400–4000 cm⁻¹ using OMNIC Spectra software. For comparison, pristine GO was also analyzed under the same conditions.

Crystalline properties and phase composition were determined using X-ray diffraction (XRD, MiniFlex, Rigaku) with CuK α radiation (λ = 1.54 Å) at room temperature. Approximately 2 g of ground GO@ZIF-8 (1:1) nanocomposite and GO were used to analyze crystallinity, phase structure, and lattice parameters. In addition, ultraviolet–visible (UV–Vis) spectroscopy (Cary 60) was employed to examine the optical properties of GO. GO was dispersed in deionized water and ultrasonicated for 30 minutes to prevent agglomeration, then placed in a quartz cuvette and scanned over the 200–800 nm wavelength range.

Removal of oil from aqueous solutions Preparation for oil-water emulsion

Sorption experiments were conducted with oil that was dissolved in water and then used as a model oily wastewater. The surfactant-stabilized synthetic oily wastewater emulsions were made by using motor oil (Shell Helix HX5 SN 10W-40) with distilled water as follows: To create a 1000 ppm stock solution, 1 mL of motor oil was mixed with 1 L of distilled water. Then, 200 mg of sodium dodecyl sulphate (SDS) as the anionic surfactant was added to the oil solution stirred for 12 hours initially [26]. If the solution had not turned completely white and cloudy by then, stirring was extended up to 24 hours until it was well-mixed. The mixture was then sonicated using a water bath sonicator for 60 minutes to obtain stable oil-water emulsions [27]. Finally, distilled water was used to dilute the oily water to produce various concentrations (10, 30, 50, 70, 90, 100, and 130 ppm). Using a UVvis spectrophotometer to measure absorbance at a wavelength of 235 nm, the amount of oil present in the feed and permeate samples was determined.

Batch adsorption study

In this experiment, the influence of several conditions

on the adsorption experiment was examined using the controlled variable approach. Different variables, including pH, contact time and initial oil concentration as shown in Table 2. The pH range was selected to explore the influence of acidity and alkalinity on the adsorption process. The pH 7 represents a neutral condition while the pH 3 and pH 10 represent acidic and alkaline conditions, respectively [28, 29]. The contact time was varied to ensure optimal adsorption equilibrium. The contact time is a crucial factor for maximizing adsorption efficiency, as longer contact times often lead to higher adsorption, but after a certain point, equilibrium is typically achieved [23]. The range of initial oil concentration was chosen to simulate different levels of oil contamination in water, allowing for the assessment of adsorption capacity under varying oil pollutant loads. The selected range is commonly used in oil-water separation studies and reflects practical concentrations found in industrial effluents, as noted in multiple studies on adsorption for wastewater treatment [30-32].

An adsorption study was performed by soaking 0.2 g of GO@ZIF-8/Al₂O₃ hollow fibre membrane into 50 mL of oily water solution. This amount of adsorbent was chosen based on studies that balance optimal adsorption efficiency with material economy. Previous works using GO-based composites have shown that this quantity is sufficient to provide maximum surface area exposure for pollutant interaction while preventing saturation [28]. Using 0.2 g helps achieve effective oil adsorption without

needing excessive adsorbent, thus making it costeffective for experimental replication [33]. Next, the solution was shaken using an orbital shaker set at 150 rpm for 8 hours.

Finally, a UV-Vis spectrophotometer operating at a wavelength of 235 nm was used to determine the oil concentration. The amount of oil adsorbed at equilibrium was calculated using q from Equation (1), and Equation (2) was used to obtain the oil removal effectiveness (percent of adsorption) [14].

Adsorption capacity (mg/g),
$$q_e = \frac{(c_o - c_e)v}{m}$$
 (1)

Removal efficiency (%) =
$$\frac{c_o - c_t}{c_o} \times 100$$
 (2)

Where C_0 (mg/L) represents the initial concentration of oil in an aqueous solution, C_t indicates the oil concentration over time, the oil concentration at equilibrium is denoted by C_e (mg/L), the volume of oil solution used was V (L), and the mass of adsorbent was m (g).

The adsorption equilibrium isotherms and kinetic models were applied for describing the mechanism of adsorption as shown in **Table 3**. The Freundlich and Langmuir isotherms explain the amount of material adsorbed per unit mass of adsorbent, whereas pseudofirst-order and pseudo-second-order kinetic models indicate the adsorption rate [34, 35].

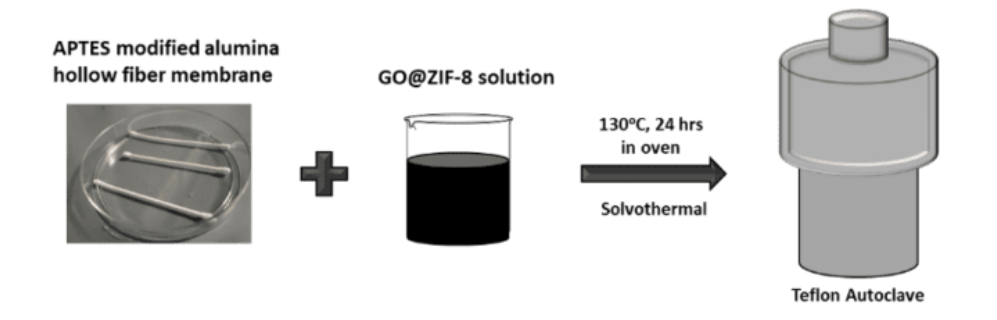


Figure 3. GO@ZIF-8/Al₂O₃ membrane in-situ solvothermal process.

 Table 2. Adsorption experiment conditions

Experiments	Initial Oil Concentration (ppm)	Adsorbent Dose (g)	Contact Time (h)	pН
Effect of pH	60	0.2	8	3, 7, 10
Effect of contact time	60	0.2	0.5-8	3
Effect of initial oil concentration	10-130	0.2	8	3

Table 3. Adsorption isotherms and kinetics models

Isotherms models	Linear equations	
Langmuir	$\frac{C_e}{q_e} = \frac{C_e}{q_m} + \frac{1}{K_L q_m}$	(3)
Freundlich	$\ln q_e = \ln K_F + \frac{1}{n} \ln C_e$	(4)
Kinetics models	Linear equations	
Pseudo-first order	$ln(q_e - q_t) = lnq_e - k_1 t$	(5)
Pseudo-second order	$\frac{t}{q_t} = \frac{1}{k_2 q_e^2} + \frac{1}{q_e} t$	(6)

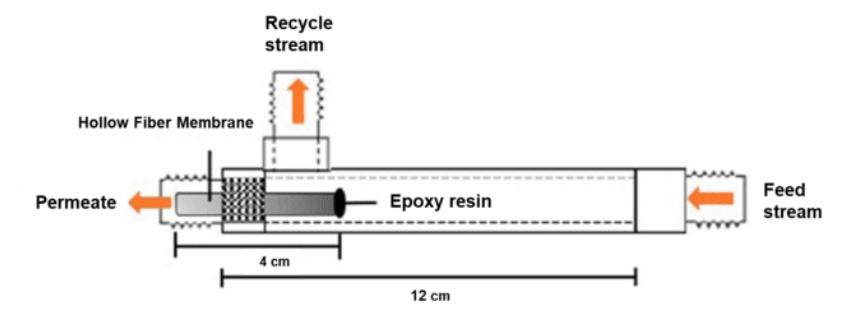


Figure 4. Hollow fibre module specifications [23]

Cross-flow filtration study

A system of crossflow filtering was applied to calculate the oil rejection and solute permeate [23]. The feed for the filtering process was produced using an oil solution with a concentration of 100 ppm. To get a significant oil rejection, the experiments were carried out at 1 bar. The concentration of oil in the permeate and in the feed solution was measured using the UV-vis spectrophotometer. Firstly, the water was allowed to penetrate the inner side of the membrane by pumping the water of the feed solution from the outer side. Then it enters via the lumen of the hollow fibre membrane to travel to the other end of the membrane, which is unsealed as shown in Figure 4. Before being collected to determine the flux and rejection, the permeates were stabilized for around 3 min. Equation (7) was used to calculate the permeate flux [23]:

$$J_{w} = \frac{V}{t \times A} \tag{7}$$

Where, $J_W = Solute flux$,

 $V = \text{volume of permeate (m}^3),$

t = time of permeate collected (h)

 $A = \text{total surface area of hollow fibre membrane (m}^2$)

For the oil rejection study, 100 ppm of diluted oil solution was used. The oil rejection was determined by using Equation (2)

Reusability study

The membrane's ability to regenerate and be reused is

crucial for long-term applications. In this study, after a 5-hour filtration period, the membrane was regenerated using a 2% wt. sodium dodecyl sulphate (SDS) solution [36, 37]. The used membrane was soaked in the SDS solution for 30 minutes and sonicated for 15 minutes before further use. The regenerated membrane was reused for five additional filtration cycles, making a total of six cycles. The rejection efficiency was tested after each cycle to assess the membrane's long-term performance [38]. The permeate flux (J, in Lm⁻²h⁻¹) and oil rejection (%) were measured in each cycle using the same calculation methods. These parameters were used to evaluate membrane reusability across six filtration cycles.

Results and Discussion Graphene oxide characterization

The structural and chemical characteristics of the synthesized graphene oxide were assessed using FTIR, UV-Vis spectroscopy, XRD, and FESEM. As shown in Figure 5, the FTIR spectrum of GO exhibits prominent absorption bands associated with oxygencontaining functional groups: O-H stretching at 3438 cm⁻¹, C=O stretching at 1704 cm⁻¹, C=C skeletal vibrations at 1640 cm⁻¹ and C-O stretching at 1117 cm⁻¹ These features confirm the introduction of polar oxygen functionalities that improve dispersibility in aqueous media [39-42]. A new peak between 1640–1500 cm⁻¹ in the GO spectrum, absent in graphite, corresponds to C=C and C-OH bending, further confirming oxidation.

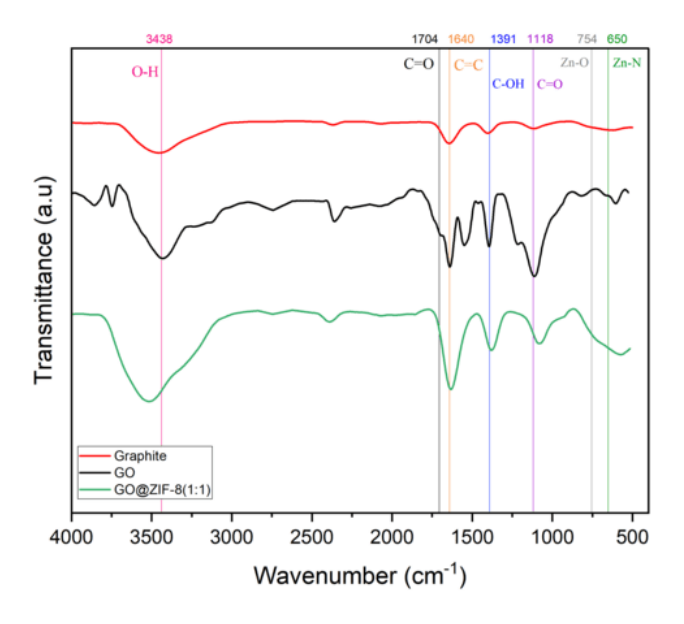


Figure 5. FTIR spectra of graphite, GO, and GO@ZIF-8(1:1) composite

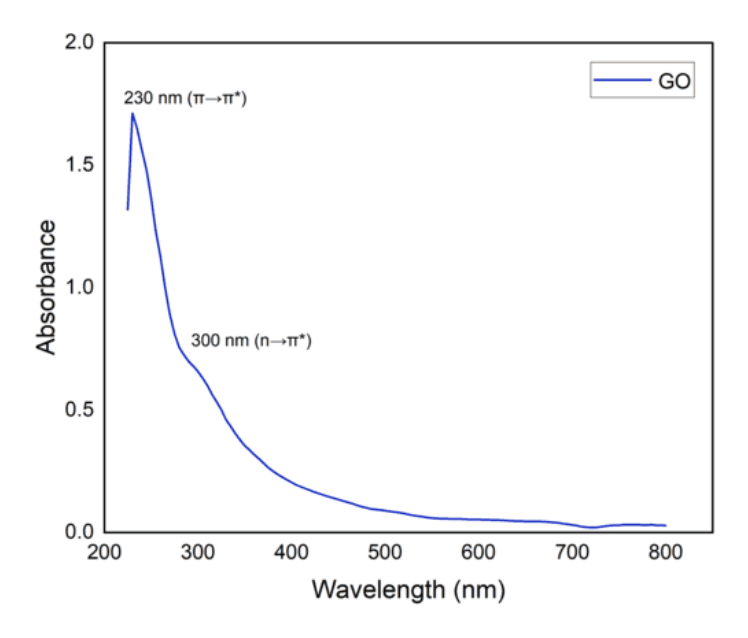


Figure 6. The UV-Vis spectrum of GO

The UV–Vis spectrum of GO (**Figure 6**) shows a strong absorption peak at \sim 230 nm ($\pi\rightarrow\pi^*$ transitions of C=C) and a weaker shoulder near 300 nm ($n\rightarrow\pi^*$ transitions of C=O), indicating disruption of the conjugated system and formation of oxygenated functional groups [43–45].

XRD analysis (**Figure 7**) reveals a diffraction peak at $2\theta = 9.51^{\circ}$, corresponding to the (001) plane and an interlayer spacing of 9.29 Å, typical of GO. A smaller peak at 42.21° indicates the (100) plane, suggesting residual graphitic ordering [14,46,47]. These results are in agreement with previous reports on GO synthesized via the modified Hummers' method [48–[50].

Malays. J. Anal. Sci. Volume 29 Number 4 (2025): 1564

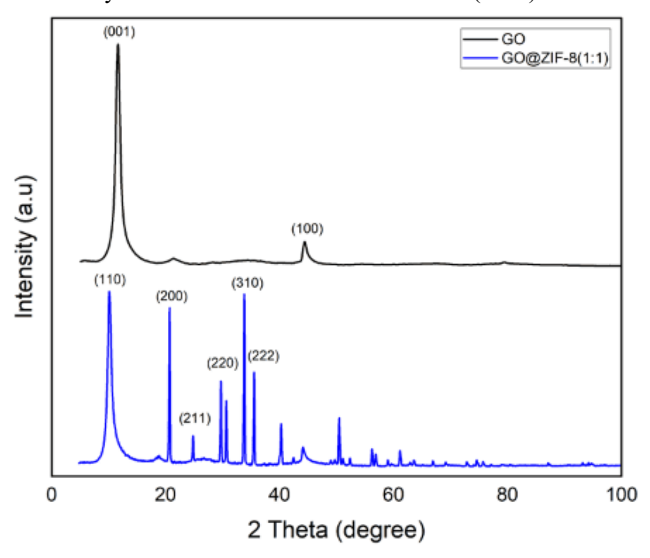


Figure 7. The XRD pattern of GO and GO@ZIF-8(1:1) composites

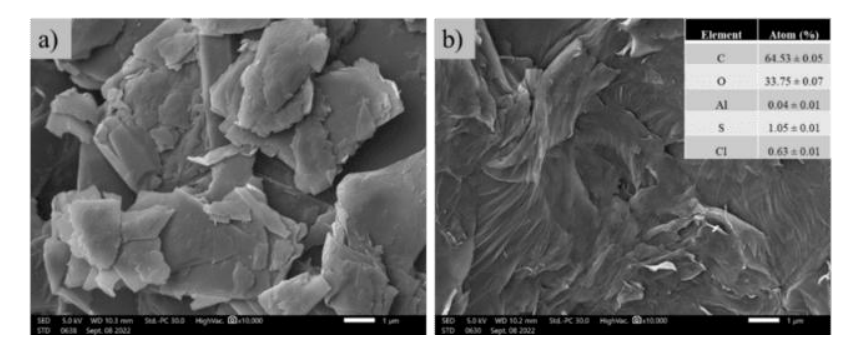


Figure 8. The SEM images of pure (a) graphite and (b) graphene oxide

Figure 8 reveals clear differences between pristine graphite and graphene oxide. The graphite microstructure exhibits structural deterioration. Graphite particles as shown in **Figure 8(a)**, exhibit compact and stacked layers with irregular surfaces [51]. Meanwhile, graphene oxide has a layered structure, allowing for the production of homogenous and ultrathin graphene films which is similar to the literature from [46, 52–54].

Based on **Figure 8**, the synthesized GO present a flakes-like structure from SEM micrographs. These films are sometimes folded, or continuous and the individual sheets' edges can be seen along with any wrinkled or kinked regions. Moreover, the EDX analysis which shows the elemental chemical compositions of the GO exhibits the presence of element carbon (C), oxygen (O), and sulphur (S) as shown in **Figure 8(b)**. The oxygen and sulphur present in the GO is due to the usage of oxidizing agent H₂SO₄ and KMnO₄ during oxidation process [55]. This proves the formation of GO where graphene layer is decorated with oxygen containing groups.

GO@ZIF-8 nanocomposites characterization

Only the GO@ZIF-8(1:1) nanocomposite was synthesized and characterized as a representative sample for structural evaluation. Figure 5 presents the FTIR spectrum of GO@ZIF-8(1:1), showing characteristic peaks that confirm successful composite formation. The spectrum demonstrated that the carboxyl group from GO was coordinated with Zn²⁺ through the elimination of the peak at 1704 cm⁻¹ [16]. As a result, as shown in **Figure 5**, the intensity of the peak at 1640 cm⁻¹ is increased and widened as the ZIF-8 content in GO@ZIF-8(1:1) composites decreases [56]. This confirmed the interaction between the GO sheets and ZIF-8 framework via coordination bonding. The peak at 750 cm⁻¹ indicated the presence of Zn-N stretching from ZIF-8, supporting the successful formation of the composite.

The FTIR spectrum retained major features of both GO and ZIF-8, confirming their integration. The widespread distribution of ZIF-8 on GO surfaces is attributed to interactions between Zn clusters and functional groups (carboxyl, epoxy) on GO [57]. It

was further demonstrated that GO@ZIF-8 was successfully synthesised when the ZIF-8 diffraction peaks interfered with the weak GO characteristic peaks [58, 59].

The XRD pattern of the GO@ZIF-8(1:1) nanocomposite is shown in Figure 7. Several strong and sharp diffraction peaks are present at 2θ values of 7.4° , 10.5° , 12.7° , 14.8° , and 18.0° , which correspond to the (011), (002), (112), (022), and (013) crystal planes of ZIF-8, respectively [14, 60, 61]. These peaks indicate a high degree of crystallinity and confirm the successful formation of ZIF-8 on the GO sheets. The disappearance of the GO peaks at ~9.5° implies disruption of the GO layered structure or complete coverage by ZIF-8, indicating successful composite formation through solvothermal synthesis.

The morphology of the GO@ZIF-8(1:1) nanocomposites was characterized using FESEM, as shown in Figure 9. The incorporation of GO nanosheets significantly influenced the formation and distribution of ZIF-8 crystals. GO served as a platform for crystal growth, and its oxygen-containing functional groups, especially carboxyl and hydroxyl interacted with Zn^{2+} ions through groups, coordination. This interaction inhibited excessive crystal growth and resulted in smaller, more uniformly dispersed ZIF-8 particles [25, 57]. The FESEM images display a lamellar, two-dimensional structure, where ZIF-8 nanocrystals are uniformly spread across the GO surface. The strong interfacial contact, facilitated by coordination interactions, contributes to improved membrane properties such as antibiofouling behaviour [62].

A dense GO layer forms between firmly adhered ZIF-8 crystals. The GO layer appeared continuous and free from visible fractures or defects. Adjusting the concentration of GO suspensions will change the extent to which the GO layer is covered. However, higher GO content leads to greater ZIF-8 coverage by the GO layer, which lowers the GO@ZIF-8 membrane permeance and reduces the "real membrane area" for flux permeation.

GO@ZIF-8 alumina hollow fibre membrane characterization

FTIR spectra of pristine alumina, ZIF-8/Al₂O₃ and GO_(1:1)@ZIF-8/Al₂O₃ composite membrane is shown in Figure 10. The GO_(1:1)@ZIF-8/Al₂O₃ spectrum displays a broad band at 3454 cm⁻¹, corresponding to O-H stretching and a reduced C=C peak at 1627 cm⁻¹, indicating surface modification after the incorporation of ZIF-8. These changes suggest successful deposition of ZIF-8 onto the GO surface, which was further attached to the alumina support [63]. The broadening of absorption bands in the $GO_{(1:1)}$ @ZIF-8/Al₂O₃ sample after **APTES** modification indicates that the ZIF-8 layer formed effectively on the membrane support. Peaks located at 1384 cm⁻¹ and 1588 cm⁻¹ are assigned to imidazole ring stretching and C=N stretching vibrations, respectively [23]. Other absorption bands appearing between 1380 cm⁻¹ and 960 cm⁻¹ are attributed to inplane bending of the imidazole ring, while the signals in the 740–609 cm⁻¹ range correspond to aromatic sp^2 C-H bending [60, 64]. Additionally, a peak near 439 cm⁻¹ confirms the Zn-N stretching, indicating the presence of ZIF-8.

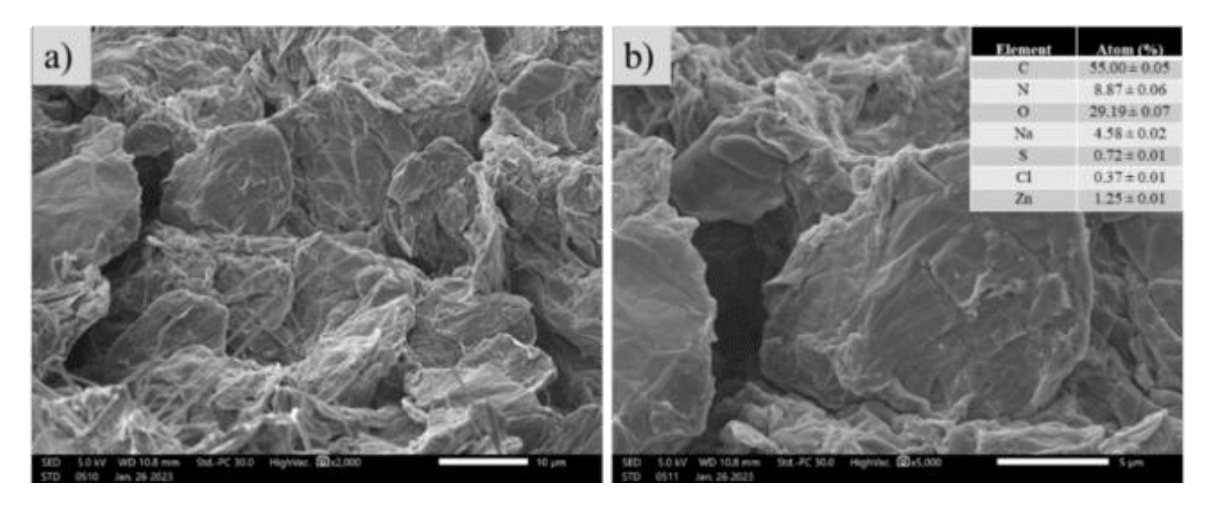
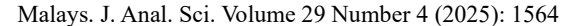


Figure 9. SEM micrograph of GO@ZIF-8(1:1) at magnification (a) x2000 and (b) x5000



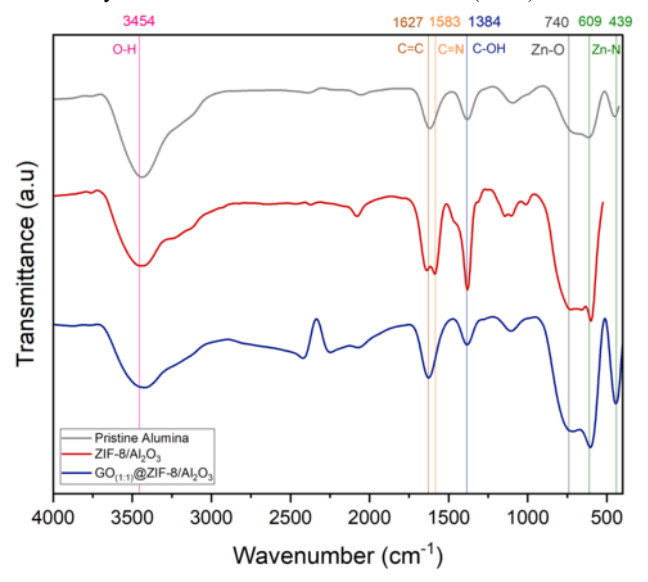


Figure 10. FTIR spectra of pristine alumina, ZIF-8/Al₂O₃ and GO_(1:1)@ZIF-8/Al₂O₃

Figures 11(a) and 11(b) show the surface and crosssection of the pristine alumina hollow fibre membrane. The membrane has a thickness of 419.26 um measured from the outer surface to the inner surface, as shown in Figure 11(b). The surface appears relatively smooth and lacks distinct crystal features as expected for an unmodified ceramic support. Internally, the membrane exhibits a welldefined asymmetric structure consisting of finger-like pores near both the shell and lumen sides, along with a sponge-like intermediate layer. This structural configuration is advantageous because it maintains good mechanical integrity while allowing controlled surface modifications [23]. The sponge-like outer region is particularly important during in-situ growth as it prevents solution penetration into the membrane core, ensuring that any deposited ZIF-8 or GO remains confined to the outer surface [23, 65]. These characteristics make the pristine alumina a stable and reliable support material for nanocomposite membrane development.

According to **Figure 12**, the surface pores of the alumina hollow fibre membrane were effectively coated with the GO@ZIF-8 nanocomposite layer. The membrane surface exhibits a combination of dodecahedral-shaped crystals and irregular rectangular domains, both of which appear anchored within the wrinkled structure of GO sheets [65]. These typical wrinkled textures are characteristic of GO and indicate that the structural integrity of the graphene oxide nanosheets was retained after the modification process [59]. Additionally, the internal morphology of the membrane reveals a distinctive brick-and-mortar pattern, where ZIF-8 crystals serve as the "bricks"

embedded between GO "mortar" layers [16]. Figures 12 and 13 provide a detailed view of both the surface and cross-section of the GO@ZIF-8/Al₂O₃ membrane. The aggregation of ZIF-8 particles caused an exceptionally rough surface to emerge on the composite membrane as the nanoparticle content increased [66]. Some disintegration of ZIF-8 crystals occurred during the APTES surface functionalization step, leading to slightly irregular dodecahedral shapes, but the core morphology of the crystals remained intact [67]. Cross-sectional images reveal that ZIF-8 particles are coated onto the GO veil-like sheets while maintaining their polyhedral shape, confirming that the crystal structure remained stable during composite preparation [68].

Moreover, altering the GO:ZIF-8 weight ratio in the precursor solution influenced surface morphology significantly. Higher GO loading led to a denser and more continuous layer of ZIF-8 crystals due to the covalent bonding and capillary forces between GO sheets, as depicted in Figures 12(c) and 12(d) [57]. These layers were not limited to a single coating, as multiple ZIF-8 particles adhered to the GO matrix, increasing dispersion across the membrane surface. The extent of coverage visibly increased with higher GO content, resulting in denser membrane coatings [16]. This laminar arrangement suggests that GO@ZIF-8 composites can produce robust and stable separation layers. In such layered systems, guest molecules migrate through interlayer nanochannels formed between adjacent GO sheets, enabling effective molecular separation sieving and performance [69].

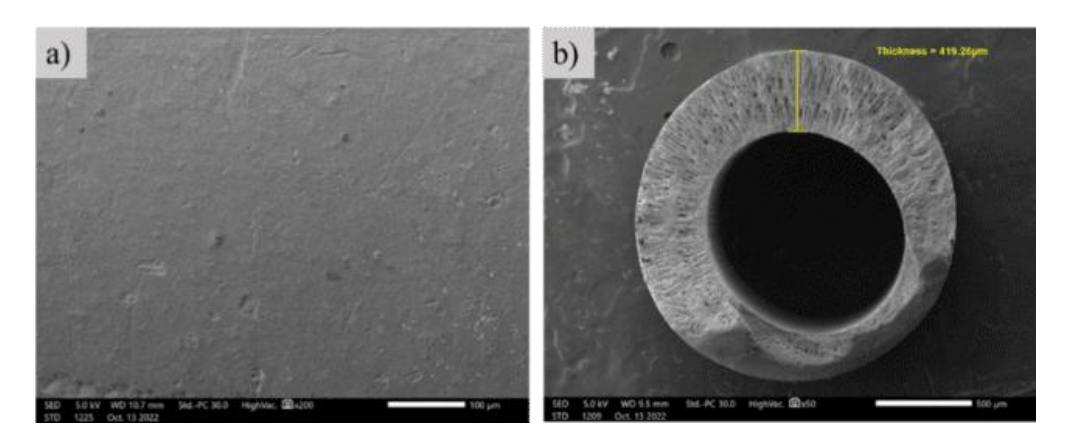


Figure 11. SEM images of pristine alumina hollow fibre a) surface, b) cross-section

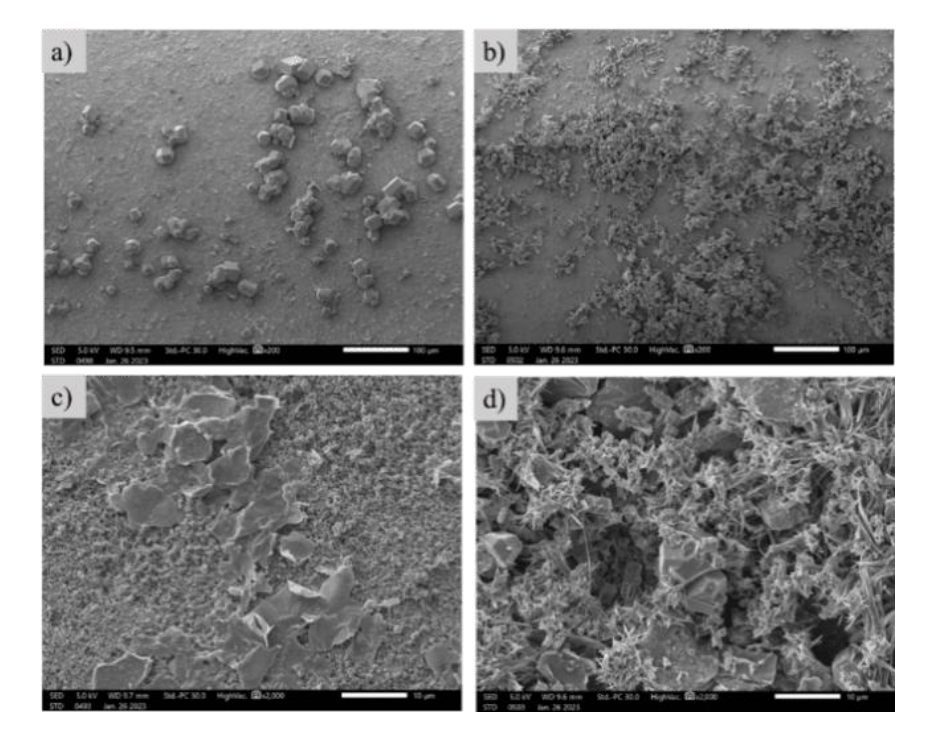


Figure 12. FESEM images of the membrane surface, $GO(_{1:1})$ @ZIF-8/Al₂O₃ at magnification (a) x200, (b) x2000 and $GO_{(2:1)}$ @ZIF-8/Al₂O₃ at magnification (b) x200, (d) x2000

The cross-sectional morphology of the $GO@ZIF-8/Al_2O_3$ membranes is illustrated in **Figure 13**. A well-defined and dense separation layer can be observed near the outer surface of the membrane. In the $GO_{(1:1)}@ZIF-8/Al_2O_3$ sample, the thickness of this layer measures approximately 13.32 μ m, while for $GO_{(2:1)}@ZIF-8/Al_2O_3$ it increases to 15.12 μ m, as shown in **Figure 13**. These variations indicate that increased GO content contributes to thicker deposition on the membrane surface. Notably, the $GO_{(1:1)}@ZIF-8/Al_2O_3$ membrane shows fewer wrinkles and reduced

particle agglomeration, which is consistent with its thinner layer and moderate composite content. In contrast, the $GO_{(2:1)}@ZIF-8/Al_2O_3$ sample displays more prominent surface roughness and thickness, which may affect membrane permeability and selectivity [16]. These morphological differences suggest that membrane performance is closely tied to the amount of GO@ZIF-8 loading. The increase in separation layer thickness is particularly important, as it influences molecular transport and adsorption pathways during separation [70].

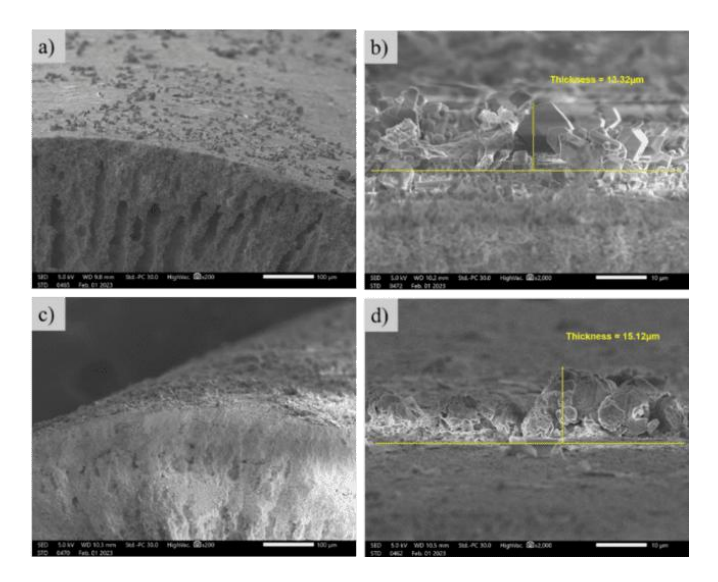


Figure 13. FESEM images of the membrane cross-section, $GO(1:1)@ZIF-8/Al_2O_3$ at magnification (a) x200, (b) x2000 and $GO(2:1)@ZIF-8/Al_2O_3$ at magnification (c) x200, (d) x2000

Study of oil emulsion adsorption Effect of pH

The influence of pH on oil emulsion removal was studied at pH 3, 7, and 10 using GO(1:1)@ZIF-8/Al₂O₃ and GO(2:1)@ZIF-8/Al₂O₃ membranes. As GO acts as an amphiphilic material with hydrophilic edges and hydrophobic basal planes [71], its performance in different pH environments was assessed to determine optimal conditions for oil adsorption. The results, shown in **Figure 14**, indicate that oil removal was highest under acidic conditions (pH 3), with the GO(2:1)@ZIF-8/Al₂O₃ membrane achieving 45.83% removal.

This enhanced performance is attributed to emulsion destabilization in acidic environments, which promotes stronger interactions between oil droplets and the membrane surface [29]. Additionally, the thicker GO@ZIF-8 layer in the GO(2:1) formulation provides a greater number of active sites for adsorption, consistent with findings that higher GO loading enhances surface functionality and adsorption capacity [72–74].

Functional group behavior also contributes to the pH-dependent performance. Under acidic conditions, partial ionization of –OH and –COOH groups reduces hydrophilicity, improving oil affinity and enabling the nanosheets to migrate toward the oil phase [75]. As pH increases, ionization decreases, weakening the membrane's affinity for oil. At pH 10, the performance declines further due to changes in surface charge, reducing the membrane's ability to bind oil molecules effectively.

Overall, acidic conditions favor oil adsorption due to enhanced emulsion destabilization and functional group interactions, while alkaline pH impairs separation efficiency.

Effect of contact time

Figure 15 shows the effect of contact time on oil adsorption. Adsorption increased gradually and reached equilibrium at around 7 hours. Membranes with higher GO content exhibited improved adsorption capacity due to a larger surface area and more functional groups, which provided additional active sites. The porous architecture and oxygen-rich surface of GO, combined with ZIF-8's crystalline structure, enhanced oil–surface interactions [76, 77].

During the initial 4 hours, the adsorption rate was rapid due to abundance of available active sites. As time progressed, these sites became saturated, resulting in a plateau in adsorption capacity and oil removal efficiency. The GO nanosheets introduced functional groups such as epoxy, hydroxyl, and carboxyl, which contributed to strong binding interactions with oil molecules [78]. At equilibrium (7 hours), the maximum adsorption capacity and oil removal efficiency were 62.5 mg/g and 41.7%, respectively.

The performance improvement with increased GO loading is attributed to the formation of layered membrane structures and enhanced surface chemistry. These findings highlight the importance of optimizing GO content for maximizing adsorption performance in oil—water separation.

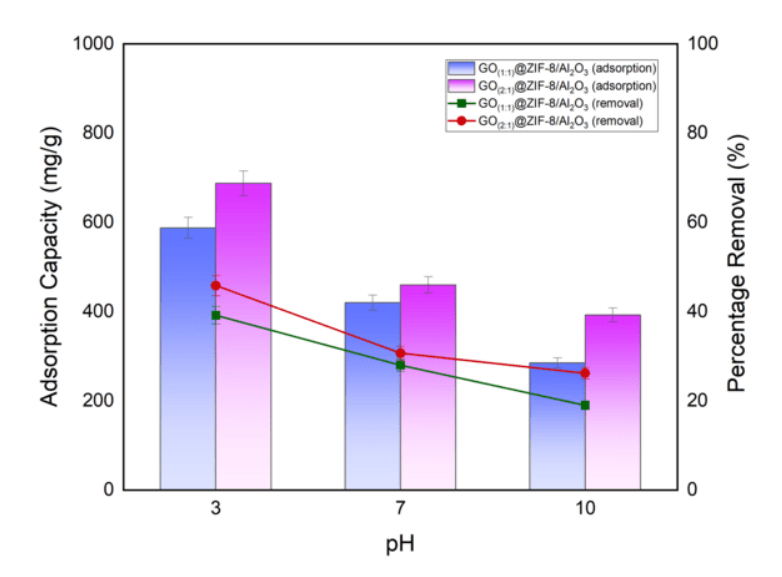


Figure 14. Effect of pH on adsorption capacity and percentage of oil removal

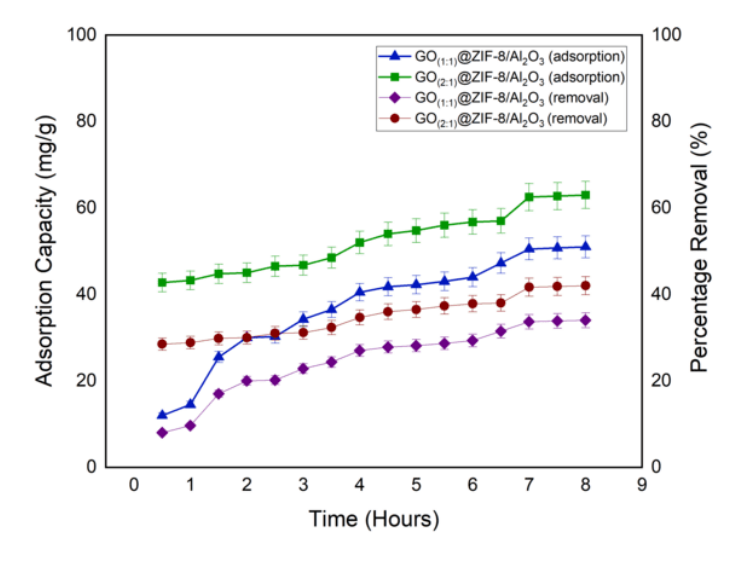


Figure 15. Effect of contact time on the oil adsorption capacity and removal percentage

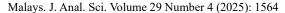
Effect of initial concentration

Figure 16 illustrates that the adsorption capacity of GO@ZIF-8/Al₂O₃ membranes increase with rising oil concentration until reaching equilibrium. As the initial oil concentration increased from 10 to 130 mg/L, the removal efficiency peaked at 53.73%, primarily due to an enhanced concentration gradient that improved mass transfer between oil molecules and membrane surfaces [79, 80].

At higher concentrations, more oil molecules interact with available active sites, but accumulation at the membrane surface may lead to pore clogging and limited diffusion into the inner structure [80]. Beyond a certain concentration, additional increases yielded

minimal or slightly reduced adsorption, likely due to site saturation or competition between oil molecules [81, 82].

This plateau reflects the finite number of adsorption sites and highlights the system's maximum uptake capacity. The performance decline at concentrations near 200 ppm suggests that the membrane approaches saturation, limiting further adsorption regardless of excess oil in the solution [82]. In conclusion, increasing initial oil concentration enhances adsorption efficiency up to a threshold. Beyond this, mass transfer limitations and surface saturation reduce further improvements in removal performance [83].



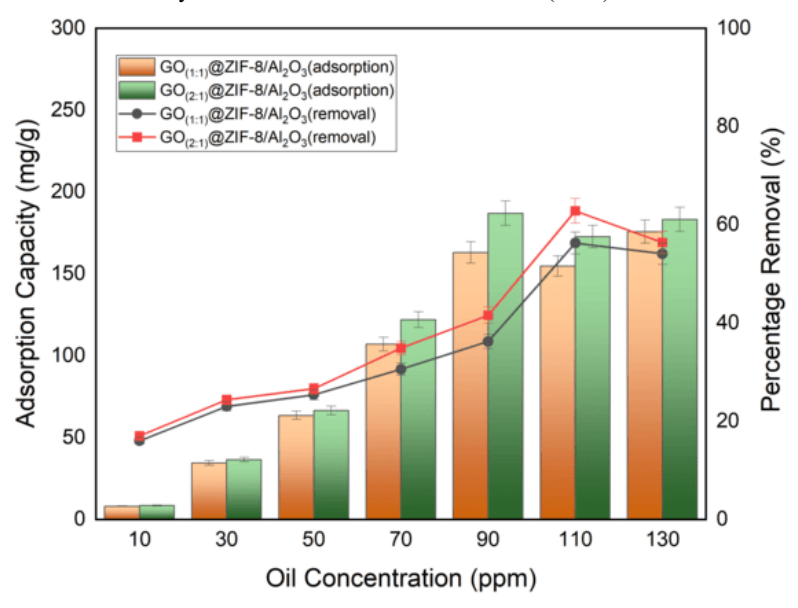


Figure 16. Effect of initial concentration on adsorption capacity and percentage of oil removal

Adsorption isotherms

Adsorption isotherm studies were conducted using the GO_(1:1)@ZIF-8/Al₂O₃ membrane to model the equilibrium interaction between oil molecules and the membrane surface. Adsorption isotherms describe the equilibrium relationship between solute concentration in the liquid phase and the amount adsorbed onto the membrane surface at constant temperature. In this study, two widely applied models, Langmuir and Freundlich isotherms were used to evaluate the adsorption performance of the GO_(1:1)@ZIF-8/Al₂O₃ membrane. The Langmuir model assumes monolayer adsorption on a homogeneous surface with identical binding sites, while the Freundlich model is empirical and describes adsorption on heterogeneous surfaces, allowing for multilayer formation [84, 85].

The Langmuir equation (Equation 3) shown in **Table 3**, includes constants such as K_L (L/mg), representing the affinity between adsorbent and adsorbate, and q_m (mg/g), the theoretical maximum adsorption capacity. A linear plot of C_e/q_e versus C_e was used to derive K_L and q_m values, yielding a regression coefficient R^2 =0.90717. However, the Langmuir constants obtained were K_L =-0.00124 and q_m =-75.1315 mg/g, which are negative and physically unrealistic. These values suggest that the Langmuir model does not adequately describe the adsorption behavior in this system, possibly due to deviation from its assumptions

under the tested conditions [58].

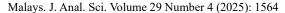
To further assess the Langmuir model, the dimensionless separation factor (R_L) was calculated using Equation (8):

$$R_L = \frac{1}{(1 - K_L C_0)} \tag{8}$$

where C_0 is the initial oil concentration (mg/L) and K_L is the Langmuir constant. The calculated R_L value of 1.12562 indicates that the adsorption was unfavorable ($R_L > 1$), further supporting the model's poor fit [86].

The Freundlich model (Equation 4), shown in **Table 3**, expresses the adsorption equilibrium through the constants K_f and n, derived from a plot of $\ln q_e$ versus $\ln C_e$. In this study, the Freundlich equation yielded an R^2 value of 0.98046, indicating a much better fit compared to the Langmuir model. The n-value obtained was 0.62983, which is less than 1, suggesting that the adsorption mechanism may involve chemisorption, where chemical interactions dominate the adsorption process [87, 88].

Overall, the Freundlich model more accurately represented the experimental data, indicating multilayer adsorption on a heterogeneous membrane surface with varied binding affinities.



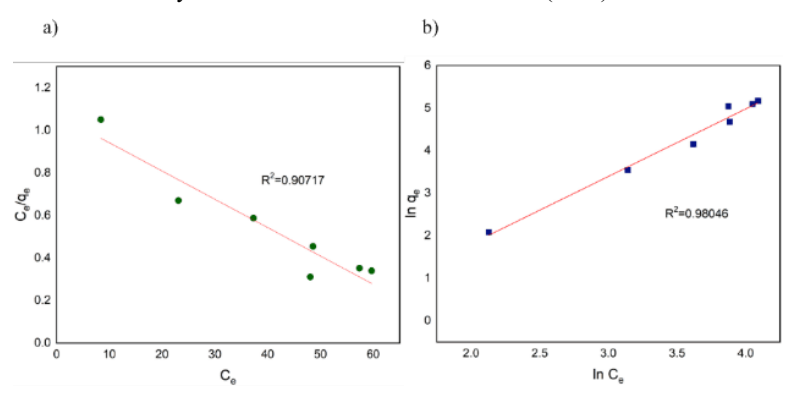


Figure 17. The (a) Langmuir isotherm and (b) Freundlich isotherm for oil adsorption on GO_(1:1)@ZIF-8/Al₂O₃

Table 4. Langmuir and Freundlich isotherm parameters for oil adsorption on GO_(1:1)@ZIF-8/Al₂O₃

Adsorption Isotherm	Isotherm Constants	Value
Langmuir	$q_{\rm m}$	-75.1315
	K_{L}	-0.00124
	$R_{ m L}$	1.12562
	\mathbb{R}^2	0.90717
Freundlich	n	0.62983
	K_{F}	0.25373
	\mathbb{R}^2	0.98046

Adsorption kinetics

Kinetic adsorption behavior was evaluated using the GO_(1:1)@ZIF-8/Al₂O₃ membrane. Adsorption kinetics describe the rate at which solutes are removed from the aqueous phase and help identify the mechanisms controlling the process. In liquid-solid systems, adsorption rates are influenced by various parameters, including adsorbent texture, pH, solute concentration, dosage, and temperature, all of which determine how quickly equilibrium is reached [89]. Several models have been developed to describe kinetic behavior, including the Elovich model, Ritchie's equation, mixed-order models, and pseudo-nth order models [90]. However, the pseudo-first order (PFO) and pseudo-second order (PSO) models remain the most widely used due to their simplicity and applicability in batch adsorption systems [91].

The PFO model, also known as the Lagergren model, assumes that the adsorption rate is proportional to the difference between the equilibrium capacity (q_e) and the adsorption capacity at time t (q_t) [86, 92]. This relationship, shown in Equation (5) in Table 3, involves the rate constant k_2 and is typically analyzed by plotting $\ln(q_e - q_t)$ against time [93].

The PSO model (Equation 6) in **Table 3**, by contrast, assumes that the rate-limiting step involves chemisorption, where electron sharing or transfer

occurs between adsorbate and adsorbent [93, 94] A plot of t/q_t versus t yields the rate constant k_2 and predicted q_e values.

To evaluate the adsorption kinetics, a batch test was performed using a 60-ppm oil emulsion. Samples were collected every 30 minutes over 8 hours, and the data were fitted to both kinetic models. **Figure 18** presents the linearized forms of PFO and PSO, while **Table 5** summarizes the kinetic parameters.

The PSO model produced a better fit, with a correlation coefficient of $R^2 = 0.98247$, significantly higher than that of the PFO model. Moreover, the experimental adsorption capacity (q_e , exp = 62.50 mg/g) closely matched the PSO-calculated value (q_e , cal = 63.5324 mg/g). These results confirm that the pseudo-second order model provides a more accurate description of the oil adsorption behaviour, likely due to chemisorption mechanisms dominating the process.

Other similar works on the oil removal are presented in **Table 6**. The adsorption capacity of the present study is comparable to other reported composite membranes. The GO@ZIF-8 modified alumina membrane also has a comparable adsorption capacity in comparison with other available alumina-based membranes.

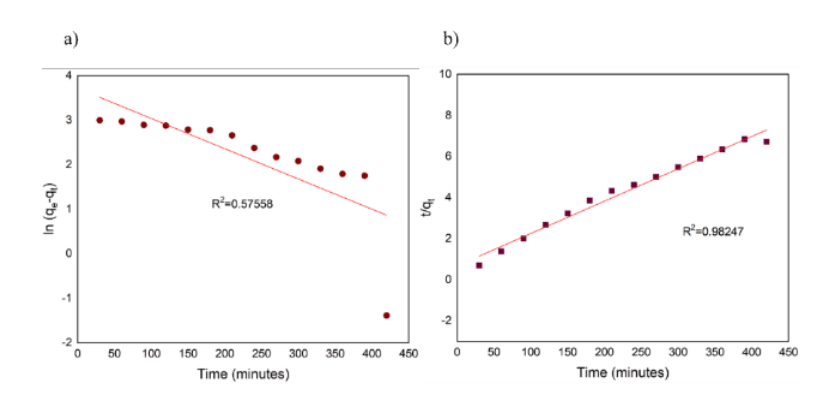


Figure 18. The plots of (a) pseudo-first order and (b) pseudo-second order kinetics for the adsorption of oil at 60 ppm on $GO_{(1:1)}$ @ZIF-8/Al₂O₃ at room temperature and pH 3

Table 5. Pseudo-first and pseudo-second order parameters for oil adsorption on GO@ZIF-8/Al₂O₃ at 60 mg/L

Adsorption kinetics	Concentrations	Kinetic Constants	Value
Pseudo-First Order	60 mg/L	q_e	41.1120
		\overline{k}_1	0.00679
		\mathbb{R}^2	0.57558
Pseudo-Second Order	60 mg/L	q_e	63.5324
		k_2	3.653e-4
		\mathbb{R}^2	0.98247

Table 6. Comparison of GO_(1:1)@ZIF-8/Al₂O₃ hollow fibre membrane adsorption capacities with the reported study for oil removal

Adsorbent	Type of Oil	Adsorption Capacity	References
		(q _{max})	
PVDF/GE	Engine oil	64.1 g/g	[95]
rGO@MF	Crude oil	5.6 g/g	[96]
PCLM	Motor oil	15.93 g/g	[97]
Polytetrafluoroethylene	Crude oil	11.7 $\mu g/cm^2$	[98]
(PTFE)			
TiO ₂ /Al ₂ O ₃ -PVDF	Oil solid	$18.57 \ \mu g/cm^2$	[99]
GO@ZIF-8/Al ₂ O ₃	Motor oil	62.50 mg/g	Present study

Oil-water separation performance Cross-flow filtration study

Crossflow filtration was conducted at 1 bar to assess the membranes' separation performance against oil emulsions. **Figure 19** shows the permeate flux and oil rejection of each membrane. The GO_(1:1)@ZIF-8/Al₂O₃ membrane exhibited the highest flux at 98.268 Lm⁻²h⁻¹, followed by the GO_(2:1)@ZIF-8/Al₂O₃ membrane at 92.147 Lm⁻²h⁻¹. In contrast, the pristine membrane recorded a significantly lower flux of 33.652 Lm⁻²h⁻¹, nearly three times less than the modified membranes.

The enhanced water permeability in GO@ZIF-8-modified membranes is attributed to the synergistic effects of GO's hydrophilic nature and ZIF-8's porous architecture. GO provides water-affinitive pathways,

while ZIF-8 offers a structured pore network that facilitates water transport and reduces mass transfer resistance [63, 100]. These features also minimize tortuosity and maintain mechanical stability [33].

ZIF-8's well-defined micropores and GO's polar functional groups promote strong interactions with water molecules, resulting in improved flux. The increased hydrophilicity of the membrane surface allows more efficient water uptake, a key advantage for filtration applications. ZIF-8 further enhances water permeability by creating additional transport channels, complementing the GO structure.

In terms of oil rejection, the modified membranes outperformed the pristine ones. GO_(2:1)@ZIF-8/Al₂O₃ showed the highest rejection at 96.32%, followed by

GO_(1:1)@ZIF-8/Al₂O₃ at 90.64%, while the pristine membrane achieved only 84.38%. The improved selectivity stems from the oxygen-containing groups on GO, which contribute to membrane hydrophilicity and stability while forming an effective barrier against oil penetration [101].

GO content also influences the trade-off between flux and rejection. Higher GO loading introduces more adsorption sites and enhances oil interaction but may reduce flux by increasing the thickness and density of the separation layer. Conversely, lower GO content can result in ZIF-8 agglomeration, reducing surface coverage and separation performance [16].

Overall, the GO_(2:1)@ZIF-8/Al₂O₃ membrane provided the best balance between oil rejection and water permeability. While the flux slightly decreased compared to the 1:1 membrane, the substantial gain in rejection efficiency supports its application for oil—water separation. These findings highlight the importance of optimizing GO content to achieve superior membrane performance.

Other similar works on the oil removal are presented in **Table 7**. The solute flux and removal efficiency of the present study are comparable to other reported composite membranes. The GO@ZIF-8/Al₂O₃ hollow fibre membrane also exhibited higher solute flux and removal efficiency in comparison with the other type of alumina membrane.

Reusability study

One important aspect of GO@ZIF-8/Al₂O₃ membranes' operational capabilities is their capacity

to be reused for water filtration [107]. To possibly reuse the membrane, membrane regeneration is important. For this study, the GO_(2:1)@ZIF-8/Al₂O₃ membrane, a composite membrane comprising graphene oxide (GO) integrated with Zeolitic Imidazolate Framework-8 (ZIF-8) was selected for the reusability study due to its superior removal efficiency in terms of permeate flux and oil rejection based on the result of the crossflow filtration study. After regeneration by SDS solution, the same settings with the pressure of 1 bar and 100 ppm oil feed solution were used for the crossflow filtrations. After six regeneration cycles using 2 wt.% SDS solution, the membrane retained 90.08% oil rejection as illustrated in Figure 20. The membrane's rejection efficiency only fell by 6.24% from the optimum results. Throughout the six cycles, the membrane continued to exhibit a stable performance in terms of oil rejection and permeate flux. At the first cycle, the oil removal efficiency reached 97.42%, with a high permeate flux of 125.798 Lm⁻²h⁻¹ the removal efficiencies of the membrane were reduced to 91.63% and 90.08% in the fifth and sixth cycles, respectively. The permeate flux decreased slightly from which is 64.064 Lm⁻²h⁻¹ at the sixth cycle of reusability. According to these findings, the synthesised composite exhibits significant possibilities and high recoverability for reuse. This proved that the GO@ZIF-8 composite is simple to regenerate, which considerably lowers the cost of materials and the synthesis procedure. The membrane surface desorbs the weakly attached oil molecules following the surfactant treatment, and the membrane once more shows its potential [107]. To conclude, the results of the regeneration study imply that the SDS solution has successfully regenerated the membrane.

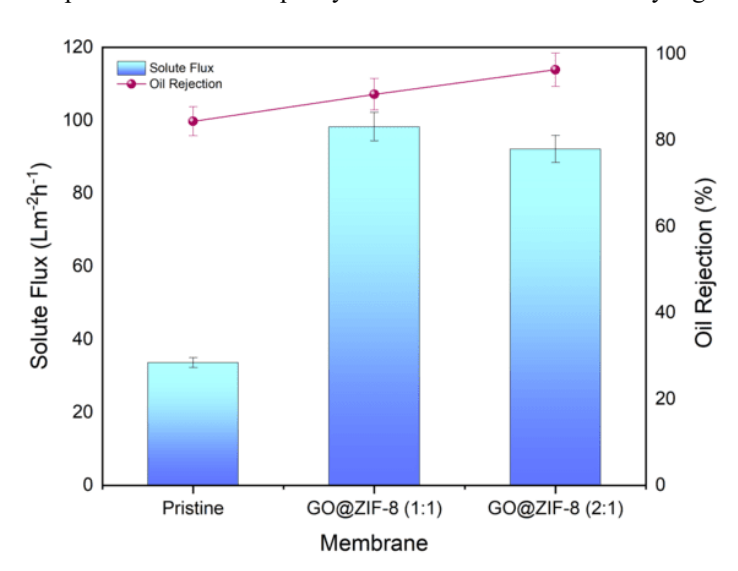


Figure 19. The solute flux and oil rejection of pristine and GO@ZIF-8 membranes

Table 7. Comparison of GO@ZIF-8/Al₂O₃ hollow fibre membrane solute flux and removal efficiency with the reported study for oil removal

Type of Water Treatment Membrane	Flux (Lm ⁻² h ⁻¹)	Removal Efficiency	References
MTES coated kaolin	80	90	[6]
TiO_2/Al_2O_3	41.8	99.1	[102]
Fenton-AC/CM	82	97	[103]
Ag-CuO-TiO ₂ /ZrO ₂	303.63	97.8	[38]
GO- Al ₂ O ₃	42	90	[104]
$\mathrm{Al_2O_3/AC}$	Not mentioned	99.02	[105]
Al_2O_3/AC	60	98.8	[106]
GO@ZIF-8/Al ₂ O ₃	92.147	96.32	Present study

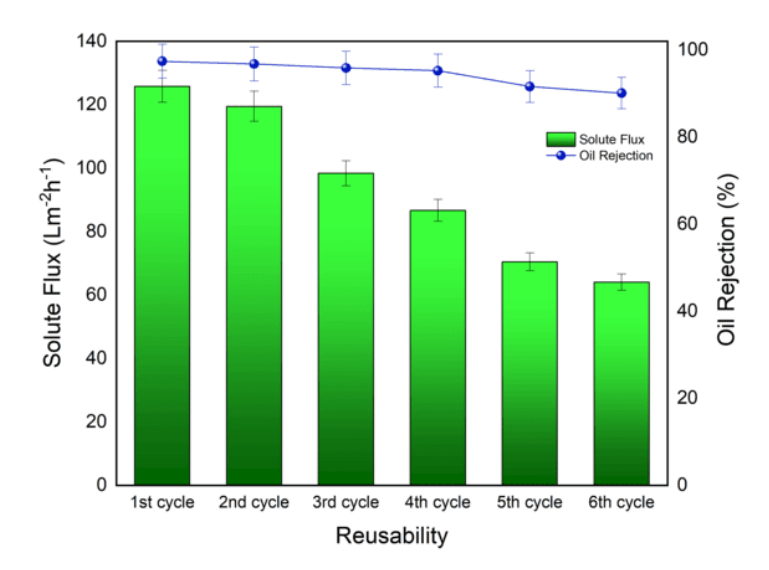


Figure 20. The solute flux and oil rejection of GO_(2:1)@ZIF-8/Al₂O₃ membrane for six cycles of reusability

Conclusion

In this study, a GO@ZIF-8 nanocomposite was successfully synthesized using a one-step in-situ solvothermal method and anchored onto an alumina hollow fibre membrane via APTES surface modification. The structural and chemical characterizations (FESEM, XRD, FTIR, and UV-Vis) confirmed successful formation of the hybrid membrane. Compared to the unmodified membrane, the GO_(2:1)@ZIF-8/Al₂O₃ formulation demonstrated superior oil adsorption performance, achieving a maximum capacity of 62.50 mg/g in batch studies and 96.32% oil rejection with a high-water flux of 92.147 Lm⁻² h⁻¹ under crossflow filtration. The adsorption behavior followed the Freundlich isotherm and pseudo-second-order kinetics, indicating a multilayer chemisorption mechanism on heterogeneous surfaces. Importantly, the membrane exhibited good durability and reusability, maintaining over 90% oil rejection after six reusability cycles, which demonstrates its suitability for long-term use. These results directly address the limitations of conventional GO

membranes, such as poor stability and low selectivity, by integrating ZIF-8 to improve both performance and membrane integrity. Overall, this research bridges a key gap in membrane technology by demonstrating a scalable fabrication strategy for producing structurally stable, high-performing GO@ZIF-8/Al₂O₃ membranes. The membrane's high removal efficiency, operational stability, and reusability highlights its potential for practical deployment in oily wastewater treatment systems, particularly in industrial applications where reliability and regeneration are essential.

Acknowledgement

This work was financially funded by the Tun Openg Chair (Sago Chair) of Universiti Malaysia Sarawak (UNI/F07/TOC/84783/2023).

References

1. Hasan, M. K., Shahriar, A., and Jim, K. U. (2019). Water pollution in Bangladesh and its impact on public health. *Heliyon*, 5(8): e02145.

- 2. Kumar Nougriaya, S., Chopra, M. K., Gupta, B., and Baredar, P. (2020). Stepped solar still: A review on designs analysis. *Materials Today: Proceedings*, 46: 5647-5660.
- 3. Chen, M., Heijman, S. G. J., and Rietveld, L. C. (2021). State-of-the-art ceramic membranes for oily wastewater treatment: Modification and application. *Membranes*, 11(11): 888.
- Kandeal, A. W., Joseph, A., Elsharkawy, M., Elkadeem, M. R., Hamada, M. A., Khalil, A., ... and Sharshir, S. W. (2022). Research progress on recent technologies of water harvesting from atmospheric air: A detailed review. Sustainable Energy Technologies and Assessments, 52: 10200.
- 5. Tanudjaja, H. J., Hejase, C. A., Tarabara, V. V., Fane, A. G., and Chew, J. W. (2019). Membrane-based separation for oily wastewater: A practical perspective. *Water Research*, 156: 347-365.
- Usman, J., Othman, M. H., Ismail, A. F., Rahman, M. A., Jaafar, J., Raji, Y. O., ... and Kurniawan, T. A. (2020). Impact of organosilanes modified superhydrophobic-superoleophilic kaolin ceramic membrane on efficiency of oil recovery from produced water. *Journal of Chemical Technology & Biotechnology*, 95(12): 3300-3315.
- Usman, J., Othman, M. H. D., Ismail, A. F., Rahman, M. A., Jaafar, J., Raji, Y. O., ... and Said, K. A. M. (2021). An overview of superhydrophobic ceramic membrane surface modification for oil-water separation. *Journal of Materials Research and Technology*, 12: 643-667.
- 8. Abuhasel, K., Kchaou, M., Alquraish, M., Munusamy, Y., and Jeng, Y. T. (2021). Oily wastewater treatment: Overview of conventional and modern methods, challenges, and future opportunities. *Water*, 13(7): 980.
- 9. Sathya, K., Nagarajan, K., Carlin Geor Malar, G., Rajalakshmi, S., and Raja Lakshmi, P. (2022). A comprehensive review on comparison among effluent treatment methods and modern methods of treatment of industrial wastewater effluent from different sources. *Applied Water Science*, 12(4): 70.
- Yalcinkaya, F., Boyraz, E., Maryska, J., and Kucerova, K. (2020). A review on membrane technology and chemical surface modification for the oily wastewater treatment. *Materials*, 13(2): 493.
- Ma, C., Li, Y., Nian, P., Liu, H., Qiu, J., and Zhang, X. (2019). Fabrication of oriented metalorganic framework nanosheet membrane coated stainless steel meshes for highly efficient oil/water separation. Separation and Purification Technology, 229: 115835.
- 12. Abdullayev, A., Bekheet, M. F., Hanaor, D. A. H., and Gurlo, A. (2019). Materials and applications

- for low-cost ceramic membranes. *Membranes*, 9(9): 105.
- 13. Kang, L., Zhao, L., Yao, S., and Duan, C. (2019). A new architecture of super-hydrophilic β-SiAlON/graphene oxide ceramic membrane for enhanced anti-fouling and separation of water/oil emulsion. *Ceramics International*, 45(13), 16717-16721.
- 14. Nikou, M., Samadi-Maybodi, A., Yasrebi, K., and Sedighi-Pashaki, E. (2021). Simultaneous monitoring of the adsorption process of two organophosphorus pesticides by employing GO/ZIF-8 composite as an adsorbent. *Environmental Technology & Innovation*, 23: 101590.
- 15. Dhaka, S., Kumar, R., Deep, A., Kurade, M. B., Ji, S. W., and Jeon, B. H. (2019). Metal-organic frameworks (MOFs) for the removal of emerging contaminants from aquatic environments. *Coordination Chemistry Reviews*, 380: 330-352.
- Yang, H., Wang, N., Wang, L., Liu, H. X., An, Q. F., and Ji, S. (2018). Vacuum-assisted assembly of ZIF-8@GO composite membranes on ceramic tube with enhanced organic solvent nanofiltration performance. *Journal of Membrane Science*, 545: 158-166.
- 17. Wang, Z., Huang, J., Mao, J., Guo, Q., Chen, Z., and Lai, Y. (2020). Metal-organic frameworks and their derivatives with graphene composites: Preparation and applications in electrocatalysis and photocatalysis. *Journal of Materials Chemistry A*, 8(6): 2934-2961.
- Zheng, Y., Zheng, S., Xue, H., and Pang, H. (2018). Metal-organic frameworks/graphene-based materials: Preparations and applications. Advanced Functional Materials, 28(47): 1804950.
- 19. Pillai, P., Dharaskar, S., Sasikumar, S., & Khalid, M. (2019). Zeolitic imidazolate framework-8 nanoparticle: A promising adsorbent for effective fluoride removal from aqueous solution. *Applied Water Science*, *9*(7): 1-12.
- Hammoud, H. M. M., & Hamzah, A. P. D. A. H. (2022). Fabrication and characterization of alumina thin film. University of Babylon.
- 21. Hummers, W. S., and Offeman, R. E. (1958). Preparation of graphitic oxide. *Journal of the American Chemical Society*, 80(6): 1339.
- Hu, Y., Wei, J., Liang, Y., Zhang, H., Zhang, X., Shen, W., and Wang, H. (2016). Zeolitic imidazolate framework/graphene oxide hybrid nanosheets as seeds for the growth of ultrathin molecular sieving membranes. *Angewandte Chemie International Edition*, 55(6): 2048-2052.
- Awang Chee, D. N. B., Aziz, F., Ismail, A. F., Mohamed Amin, M. A. B., and Abdullah, M. S. (2021). Dual-function ZIF-8 membrane supported on alumina hollow fiber membrane for

- copper(II) removal. *Journal of Environmental Chemical Engineering*, 9(4): 105343.
- Ahmad, N., Samavati, A., Nordin, N. A. H. M., Jaafar, J., Ismail, A. F., and Malek, N. A. N. N. (2020). Enhanced performance and antibacterial properties of amine-functionalized ZIF-8decorated GO for ultrafiltration membrane. Separation and Purification Technology, 239: 116554.
- 25. Li, D., and Xu, F. (2021). Removal of Cu(II) from aqueous solutions using ZIF-8@GO composites. *Journal of Solid State Chemistry*, 302: 122406.
- Raji, Y. O., Othman, M. H. D., Nordin, N. A. H. S. M., Kurniawan, T. A., Ismail, A. F., Rahman, M. A., ... and Farag, T. M. (2021). Wettability improvement of ceramic membrane by intercalating nano-Al2O3 for oil and water separation. Surfaces and Interfaces, 25: 101178.
- 27. Zhong, L., Sun, C., Yang, F., and Dong, Y. (2021). Superhydrophilic spinel ceramic membranes for oily emulsion wastewater treatment. *Journal of Water Process Engineering*, 42: 102161.
- 28. Li, H., Cheng, Y., Li, J., Li, T., Zhu, J., Deng, W., ... and He, D. (2022). Preparation and adsorption performance study of graphene quantum dots@ ZIF-8 composites for highly efficient removal of volatile organic compounds. *Nanomaterials*, 12(22): 4008.
- Mottaghi, H., Mohammadi, Z., Abbasi, M., Tahouni, N., and Panjeshahi, M. H. (2021). Experimental investigation of crude oil removal from water using polymer adsorbent. *Journal of Water Process Engineering*, 40: 101959.
- Diraki, A., Mackey, H. R., McKay, G., and Abdala, A. (2019). Removal of emulsified and dissolved diesel oil from high salinity wastewater by adsorption onto graphene oxide. *Journal of Environmental Chemical Engineering*, 7(3): 103106.
- Ewis, D., Benamor, A., Ba-Abbad, M. M., Nasser, M., El-Naas, M., and Qiblawey, H. (2020). Removal of oil content from oil-water emulsions using iron oxide/bentonite nano adsorbents. *Journal of Water Process Engineering*, 38: 101583.
- 32. Diraki, A., Mackey, H., McKay, G., and Abdala, A. A. (2018). Removal of oil from oil—water emulsions using thermally reduced graphene and graphene nanoplatelets. *Chemical Engineering Research and Design*, 137: 47-59.
- 33. Masibi, E. G., Makhetha, T. A., and Moutloali, R. M. (2022). Effect of the incorporation of ZIF-8@GO into the thin-film membrane on salt rejection and BSA fouling. *Membranes*, *12*(4): 1-23.
- Khan, I. U., Othman, M. H. D., Jilani, A., Ismail,
 A. F., Hashim, H., Jaafar, J., ... and Rehman, G.
 U. (2018). Economical, environmental friendly

- synthesis, characterization for the production of zeolitic imidazolate framework-8 (ZIF-8) nanoparticles with enhanced CO2 adsorption. *Arabian Journal of Chemistry*, 11(7): 1072-1083.
- 35. Simonin, J. P. (2016). On the comparison of pseudo-first order and pseudo-second order rate laws in the modeling of adsorption kinetics. *Chemical Engineering Journal*, 300: 254-263.
- Lv, Z., Zhang, S., Jiao, W., Zuo, X., Zhang, Y., and Liu, Y. (2023). High-efficiency cleaning technology and lifespan prediction for the ceramic membrane treating secondary treated effluent. Water Science and Technology, 88(1): 321-338.
- 37. Gruskevica, K., and Mezule, L. (2021). Cleaning methods for ceramic ultrafiltration membranes affected by organic fouling. *Membranes*, 11(2): 1–15.
- 38. Avornyo, A. J., Thanigaivelan, A., Krishnamoorthy, R., Hassan, S. W., and Banat, F. (2023). Ag-CuO-decorated ceramic membranes for effective treatment of oily wastewater. Membranes, 13(2): 176.
- Junaidi, N. F. D., Othman, N. H., Fuzil, N. S., Shayuti, M. S. M., Alias, N. H., Shahruddin, M. Z., ... and Aba, N. D. (2021). Recent development of graphene oxide-based membranes for oil water separation: A review. Separation and Purification Technology, 258: 118000.
- Sastry, S. S. M., Panjikar, S., and Raman, R. S. (2021). Graphene and graphene oxide as a support for biomolecules in the development of biosensors. *Nanotechnology, Science and Applications*, 14: 197-220.
- 41. Tiwari, S. K., Sahoo, S., Wang, N., and Huczko, A. (2020). Graphene research and their outputs: Status and prospect. *Journal of Science: Advanced Materials and Devices, 5*(1): 10-29.
- 42. Yu, W., Sisi, L., Haiyan, Y., and Jie, L. (2020). Progress in the functional modification of graphene/graphene oxide: A review. *RSC Advances*, 10(26): 15328-15345.
- 43. Trikkaliotis, D. G., Christoforidis, A. K., Mitropoulos, A. C., and Kyzas, G. Z. (2021). Graphene oxide synthesis, properties and characterization techniques: A comprehensive review. *ChemEngineering*, *5*(3): 64.
- 44. Trikkaliotis, D. G., Mitropoulos, A. C., and Kyzas, G. Z. (2020). Low-cost route for top-down synthesis of over- and low-oxidized graphene oxide. *Colloids and Surfaces A: Physicochemical and Engineering Aspects*, 600: 124928.
- 45. Chen, H., Du, W., Liu, J., Qu, L., and Li, C. (2019). Efficient room-temperature production of high-quality graphene by introducing removable oxygen functional groups to the precursor. *Chemical Science*, 10(4): 1244-1253.

- 46. Abaszade, R. G. (2022). Synthesis and analysis of flakes graphene oxide. *Journal of Optoelectronics and Biomedical Materials*, 14(3): 107-114.
- Guliyeva, N. A., Abaszade, R. G., Khanmammadova, E. A., and Azizov, E. M. (2023). Synthesis and analysis of nanostructured graphene oxide. *Journal of Optoelectronics and Biomedical Materials*, 15(1): 23-30.
- 48. Al-Gaashani, R., Najjar, A., Zakaria, Y., Mansour, S., and Atieh, M. A. (2019). XPS and structural studies of high quality graphene oxide and reduced graphene oxide prepared by different chemical oxidation methods. *Ceramics International*, 45(11): 14439-14448.
- 49. Ain, Q. T., Haq, S. H., Alshammari, A., Al-Mutlaq, M. A., and Anjum, M. N. (2019). The systemic effect of PEG-nGO-induced oxidative stress in vivo in a rodent model. *Beilstein Journal of Nanotechnology*, 10(1): 901-911.
- Kumar, A., Sadanandhan, A. M., and Jain, S. L. (2019). Silver doped reduced graphene oxide as a promising plasmonic photocatalyst for oxidative coupling of benzylamines under visible light irradiation. *New Journal of Chemistry*, 43(23): 9116-9122.
- 51. Zhang, Y., Fang, Z., Zhao, S., Wei, M., Wu, X., and Sun, L. (2020). An experimental study on the wall collision of micro-sized graphite particles by high-speed photomicrography. *Progress in Nuclear Energy*, 125: 103391.
- 52. Adetayo, A., and Runsewe, D. (2019). Synthesis and fabrication of graphene and graphene oxide: A review. *Open Journal of Composite Materials*, 9(2): 207-229.
- 53. Benzait, Z., Chen, P., and Trabzon, L. (2021). Enhanced synthesis method of graphene oxide. *Nanoscale Advances*, *3*(1): 223-230.
- 54. Chen, X., Qu, Z., Liu, Z., and Ren, G. (2022). Mechanism of oxidization of graphite to graphene oxide by the Hummers method. *ACS Omega*, 7(27): 23503-23510.
- 55. Abaszade, R. G., Mamedova, S. A., Agayev, F. G., Budzulyak, S. I., Kapush, O. A., Mamedova, M. A., ... and Kotsyubynsky, V. O. (2021). Synthesis and characterization of graphene oxide flakes for transparent thin films. *Physics and Chemistry of Solid State*, 22(3): 595-601.
- Zhu, T., Xu, S., Yu, F., Yu, X., and Wang, Y. (2020). ZIF-8@GO composites incorporated polydimethylsiloxane membrane with prominent separation performance for ethanol recovery. *Journal of Membrane Science*, 598: 117681.
- 57. Zhu, Q., Zhuang, W., Chen, Y., Wang, Z., Villacorta Hernandez, B., Wu, J., ... and Zhu, Z. (2018). Nano-biocatalysts of Cyt c@ ZIF-8/GO composites with high recyclability via a de novo approach. ACS Applied Materials &

- Interfaces, 10(18): 16066-16076.
- 58. Hoseinzadeh, H., Hayati, B., Shahmoradi Ghaheh, F., Seifpanahi-Shabani, K., and Mahmoodi, N. M. (2021). Development of room temperature synthesized and functionalized metal-organic framework/graphene oxide composite and pollutant adsorption ability. *Materials Research Bulletin*, 142: 111408.
- Makhetha, T. A., Ray, S. C., and Moutloali, R. M. (2020). Zeolitic imidazolate framework-8-encapsulated nanoparticle of Ag/Cu composites supported on graphene oxide: Synthesis and antibacterial activity. ACS Omega, 5(17): 9626-9640
- Tuncel, D., and Ökte, A. N. (2021). Improved adsorption capacity and photoactivity of ZnO-ZIF-8 nanocomposites. *Catalysis Today*, 361: 191-197.
- 61. Li, D., Liu, H., Niu, C., Yuan, J., and Xu, F. (2019). mpg-C₃N₄-ZIF-8 composites for the degradation of tetracycline hydrochloride using visible light. *Water Science and Technology*, 80(11): 2206-2217.
- 62. Wang, X., Zhao, Y., Tian, E., Li, J., and Ren, Y. (2018). Graphene oxide-based polymeric membranes for water treatment. *Advanced Materials Interfaces*, 5(15): 1701427.
- 63. Makhetha, T. A., and Moutloali, R. M. (2020). Stable zeolitic imidazolate framework-8 supported onto graphene oxide hybrid ultrafiltration membranes with improved fouling resistance and water flux. *Chemical Engineering Journal Advances*, 1: 100005.
- 64. Biata, N. R., Jakavula, S., Mpupa, A., Moutloali, R. M., and Nomngongo, P. N. (2022). Recovery of palladium and gold from PGM ore and concentrates using ZnAl-layered double hydroxide@zeolitic imidazolate framework-8 nanocomposite. *Separations*, 9(10): 274.
- 65. Ahmad, N., Nordin, N. A. H. M., Jaafar, J., Ismail, A. F., and Ramli, M. K. N. B. (2021). Significant improvement in antibacterial property of ZIF-8 decorated graphene oxide by postsynthetic modification process. *Journal of Environmental Chemical Engineering*, 9(5): 105887.
- 66. Chen, F., Dong, S., Wang, Z., Xu, J., Xu, R., and Wang, J. (2020). Preparation of mixed matrix composite membrane for hydrogen purification by incorporating ZIF-8 nanoparticles modified with tannic acid. *International Journal of Hydrogen Energy*, 45(12): 7444-7454.
- 67. Wei, N., Zheng, X., Ou, H., Yu, P., Li, Q., and Feng, S. (2019). Fabrication of an aminemodified ZIF-8@GO membrane for higherficiency adsorption of copper ions. *New Journal of Chemistry*, 43(14): 5603-5610.
- 68. Li, C. R., Hai, J., Fan, L., Li, S. L., Wang, B. D.,

- and Yang, Z. Y. (2019). Amplified colorimetric detection of Ag⁺ based on Ag⁺-triggered peroxidase-like catalytic activity of ZIF-8/GO nanosheets. *Sensors and Actuators B: Chemical*, 284: 213-219.
- 69. Su, P., Wang, F., Li, Z., Tang, C. Y., and Li, W. (2020). Graphene oxide membranes: Controlling their transport pathways. *Journal of Materials Chemistry A*, 8(31): 15319-15340.
- Wang, Y., Li, L., Zhang, X., Li, J., Wang, J., and Li, N. (2020). Polyvinylamine/amorphous metakaolin mixed-matrix composite membranes with facilitated transport carriers for highly efficient CO₂/N₂ separation. *Journal of Membrane Science*, 599: 117828.
- McCoy, T. M., Turpin, G., Teo, B. M., and Tabor, R. F. (2019). Graphene oxide: A surfactant or particle? *Current Opinion in Colloid & Interface Science*, 39: 98-109.
- Cao, J., Su, Y., Liu, Y., Guan, J., He, M., Zhang, R., and Jiang, Z. (2018). Self-assembled MOF membranes with underwater superoleophobicity for oil/water separation. *Journal of Membrane Science*, 566: 268-277.
- 73. Efome, J. E., Rana, D., Matsuura, T., and Lan, C. Q. (2019). Effects of operating parameters and coexisting ions on the efficiency of heavy metal ions removal by nano-fibrous metal-organic framework membrane filtration process. *Science of the Total Environment*, 674: 355-362.
- Abu-Nada, A., Abdala, A., and McKay, G. (2021). Isotherm and kinetic modeling of strontium adsorption on graphene oxide. Nanomaterials, 11(11): 1-11.
- 75. Javadian, S., Khalilifard, M., and Sadrpoor, S. M. (2019). Functionalized graphene oxide with coreshell of Fe₃O₄@oleic acid nanospheres as a recyclable demulsifier for effective removal of emulsified oil from oily wastewater. *Journal of Water Process Engineering*, 32: 100961.
- Kubra, K. T., Salman, M. S., and Hasan, M. N. (2021). Enhanced toxic dye removal from wastewater using biodegradable polymeric natural adsorbent. *Journal of Molecular Liquids*, 328: 115468.
- 77. Ni, W., Xiao, X., Geng, W., Zhang, L., Li, Y., and Li, N. (2021). Controllable preparation of aminofunctionalized ZIF-8: A functionalized MOF material for adsorbing Congo Red and Eriochrome Black T in aqueous solution. *JCIS Open*, 3: 100018.
- Mo, Z., Tai, D. Z., Zhang, H., and Shahab, A. (2022). A comprehensive review on the adsorption of heavy metals by zeolite imidazole framework (ZIF-8) based nanocomposite in water. *Chemical Engineering Journal*, 443: 136320.
- 79. Abadikhah, H., Zou, C. N., Hao, Y. Z., Wang, J.

- W., Lin, L., Khan, S. A., ... and Agathopoulos, S. (2018). Application of asymmetric Si₃N₄ hollow fiber membrane for cross-flow microfiltration of oily wastewater. *Journal of the European Ceramic Society*, 38(13): 4384-4394.
- Khalifa, R. E., Omer, A. M., Tamer, T. M., Ali, A. A., Ammar, Y. A., and Eldin, M. S. M. (2019). Efficient eco-friendly crude oil adsorptive chitosan derivatives: Kinetics, equilibrium and thermodynamic studies. *Desalination and Water Treatment*, 159: 269-281.
- 81. Uddin, M. J., Ampiaw, R. E., and Lee, W. (2021). Adsorptive removal of dyes from wastewater using a metal-organic framework: A review. *Chemosphere*, 284: 131314.
- 82. Katheresan, V., Kansedo, J., and Lau, S. Y. (2018). Efficiency of various recent wastewater dye removal methods: A review. *Journal of Environmental Chemical Engineering*, 6(4): 4676-4697.
- 83. Fathy, M., El-Sayed, M., Ramzi, M., and Abdelraheem, O. H. (2018). Adsorption separation of condensate oil from produced water using ACTF prepared of oil palm leaves by batch and fixed bed techniques. *Egyptian Journal of Petroleum*, 27(3): 319-326.
- 84. Mahmoodi, N. M., Taghizadeh, M., and Taghizadeh, A. (2019). Activated carbon/metalorganic framework composite as a bio-based novel green adsorbent: Preparation and mathematical pollutant removal modeling. *Journal of Molecular Liquids*, 277: 310-322.
- 85. Ragadhita, R., and Nandiyanto, A. B. D. (2022). Curcumin adsorption on zinc imidazole framework-8 particles: Isotherm adsorption using Langmuir, Freundlich, Temkin, and Dubinin-Radushkevich models. *Journal of Engineering Science and Technology*, 17(2): 1078-1089.
- Musah, M., Azeh, Y., Mathew, J., Umar, M., Abdulhamid, Z., and Muhammad, A. (2022). Adsorption kinetics and isotherm models: A review. *Caliphate Journal of Science and Technology*, 4(1): 20-26.
- 87. Awwad, A. M., Amer, M. W., and Al-aqarbeh, M. M. (2020). TiO₂-kaolinite nanocomposite prepared from the Jordanian kaolin clay: Adsorption and thermodynamics of Pb(II) and Cd(II) ions in aqueous solution. *Chemical International*, 6(4): 168-178.
- 88. Alasadi, A. M., Khaili, F. I., and Awwad, A. M. (2019). Adsorption of Cu(II), Ni(II) and Zn(II) ions by nano kaolinite: Thermodynamics and kinetics studies. *Chemical International*, *5*(4): 258-268.
- Moussout, H., Ahlafi, H., Aazza, M., and Maghat, H. (2018). Critical of linear and nonlinear equations of pseudo-first order and pseudosecond order kinetic models. *Karbala*

- International Journal of Modern Science, 4(2): 244-254.
- 90. Wang, J., and Guo, X. (2020). Adsorption kinetic models: Physical meanings, applications, and solving methods. *Journal of Hazardous Materials*, 390: 122156.
- 91. Son, H., and An, B. (2022). Investigation of adsorption kinetics for per- and poly-fluoroalkyl substances (PFAS) adsorption onto powder activated carbon (PAC) in the competing systems. *Water, Air, & Soil Pollution*, 233(4): 129.
- 92. Sahoo, T. R., and Prelot, B. (2020). Adsorption processes for the removal of contaminants from wastewater: The perspective role of nanomaterials and nanotechnology. In Nanomaterials for the Detection and Removal of Wastewater Pollutants. Elsevier Inc. pp. 161-222.
- Revellame, E. D., Fortela, D. L., Sharp, W., Hernandez, R., and Zappi, M. E. (2020). Adsorption kinetic modeling using pseudo-first order and pseudo-second order rate laws: A review. Clean Engineering and Technology, 1: 100032.
- 94. Edet, U. A., and Ifelebuegu, A. O. (2020). Kinetics, isotherms, and thermodynamic modeling of the adsorption of phosphates from model wastewater using recycled brick waste. *Processes*, 8(6): 665.
- 95. Zhang, T., Xiao, C., Zhao, J., Liu, X., Ji, D., and Zhang, H. (2021). One-step facile fabrication of PVDF/graphene composite nanofibrous membrane with enhanced oil affinity for highly efficient gravity-driven emulsified oil/water separation and selective oil absorption. Separation and Purification Technology, 254: 117576.
- Ahmed, R. M. G., Anis, B., and Khalil, A. S. G. (2021). Facile surface treatment and decoration of graphene-based 3D polymeric sponges for high performance separation of heavy oil-in-water emulsions. *Journal of Environmental Chemical Engineering*, 9(2): 105087.
- 97. Zhang, T., Yang, R., Zhang, X., Yin, X., Tian, H., and Zhu, L. (2020). Preparation, oil adsorption behavior, and mechanism of micro/nanofibrous polycaprolactone membrane prepared through solution blow spinning. *Polymer Advanced Technologies*, 31(4): 686-698.
- 98. Zhang, B., Yu, S., Zhu, Y., Shen, Y., Gao, X., Shi, W., and Tay, J. H. (2020). Adsorption mechanisms of crude oil onto polytetrafluoroethylene membrane: Kinetics and

- isotherm, and strategies for adsorption fouling control. *Separation and Purification Technology*, 235: 116212.
- 99. Yi, X., Zhu, Y., Wang, D., Yang, F., Wang, Y., and Shi, W. (2018). Adsorption mechanism of oil-inwater on a TiO₂/Al₂O₃-polyvinylidene fluoride (PVDF) ultrafiltration membrane. *Langmuir*, 34(34): 9907-9916.
- 100.Zhao, Y., Wu, M., Guo, Y., Mamrol, N., Yang, X., Gao, C., and Van der Bruggen, B. (2021). Metalorganic framework-based membranes for selective separation of target ions. *Journal of Membrane Science*, 634: 119407.
- 101. Elhenawy, S., Khraisheh, M., Almomani, F., and Hassan, M. K. (2021). Recent developments and advancements in graphene-based technologies for oil spill cleanup and oil—water separation processes. *Nanomaterials*, 12(1): 87.
- 102.Zhang, D., Wang, G., Zhi, S., Xu, K., Zhu, L., Li, W., ... and Xue, Q. (2018). Superhydrophilicity and underwater superoleophobicity TiO₂/Al₂O₃ composite membrane with ultra low oil adhesion for highly efficient oil-in-water emulsions separation. *Applied Surface Science*, 458: 157-165
- 103.Mu, H., Qiu, Q., Cheng, R., Qiu, L., Xie, K., Gao, M., and Liu, G. (2021). Adsorption-enhanced ceramic membrane filtration using Fenton oxidation for advanced treatment of refinery wastewater: treatment efficiency and membrane-fouling control. *Membranes*, 11(9): 651.
- 104.Othman, N. H., Alias, N. H., Shahruddin, M. Z., Hussein, S. N. C. M., and Dollah, A. (2017). Supported graphene oxide hollow fibre membrane for oily wastewater treatment. AIP Conference Proceedings, 1901: 1-7.
- 105.Kayvani Fard, A., Bukenhoudt, A., Jacobs, M., McKay, G., and Atieh, M. A. (2018). Novel hybrid ceramic/carbon membrane for oil removal. *Journal of Membrane Science*, 559: 42-53.
- 106.Manawi, Y., Hussien, M., Buekenhoudt, A., Zekri, A., Al-Sulaiti, H., Lawler, J., and Kochkodan, V. (2022). New ceramic membrane for Phosphate and oil removal. *Journal of Environmental Chemical Engineering*, 10(1): 106916.
- 107. Sutrisna, P. D., Kurnia, K. A., Siagian, U. W. R., Ismadji, S., and Wenten, I. G. (2022). Membrane fouling and fouling mitigation in oil—water separation: A review. *Journal of Environmental Chemical Engineering*, 10(3): 107532.